Title

Recent Progress on Topological Structures in Ferroic Thin Films and Heterostructures

Journal

Advanced Materials, 33(6)

ISSN

0935-9648

Authors

Chen, Shanquan

Yuan, Shuai

Hou, Zhipeng

et al.

Publication Date

2021-02-01

DOI

10.1002/adma.202000857

Peer reviewed

ADVANCED MATERIALS
www.advmat.de

Recent Progress on Topological Structures in Ferroic Thin Films and Heterostructures

Shanquan Chen, Shuai Yuan, Zhipeng Hou, Yunlong Tang, Jinping Zhang, Tao Wang, Kang Li, Weiwei Zhao, Xingjun Liu, Lang Chen, Lane W. Martin, and Zuhuang Chen**

Topological spin/polarization structures in ferroic materials continue to draw great attention as a result of their fascinating physical behaviors and promising applications in the field of high-density nonvolatile memories as well as future energy-efficient nanoelectronic and spintronic devices. Such developments have been made, in part, based on recent advances in theoretical calculations, the synthesis of high-quality thin films, and the characterization of their emergent phenomena and exotic phases. Herein, progress over the last decade in the study of topological structures in ferroic thin films and heterostructures is explored, including the observation of topological structures and control of their structures and emergent physical phenomena through epitaxial strain, layer thickness, electric, magnetic fields, etc. First, the evolution of topological spin structures (e.g., magnetic skyrmions) and associated functionalities (e.g., topological Hall effect) in magnetic thin films and heterostructures is discussed. Then, the exotic polar topologies (e.g., domain walls, closure domains, polar vortices, bubble domains, and polar skyrmions) and their emergent physical properties in ferroelectric oxide films and heterostructures are explored. Finally, a brief overview and prospectus of how the field may evolve in the coming years is provided.

1. Introduction

The 2016 Nobel Prize in physics was awarded to David Thouless, John Kosterlitz, and Duncan Haldane for "theoretical discoveries of topological phase transitions and topological phases of matter," which highlights the role and significance of topology in materials science and physics. Topology is an important branch of mathematics that studies properties of spaces invariant under smooth continuous deformations. The concept of topology was introduced to study various exotic states of condensed matter, especially the topological structure associated with exotic polarization/spin configuration in real space and topological phenomenon in reciprocal- or momentum-space (e.g., topological insulators).[1–3] Over the past decade, owing to precise theoretical predictions and experimental advances in synthesis and characterization, more and more intriguing topological structures have been discovered; thus opening up a new world of materials science and the fundamental physics.[4] For instance, magnetic skyrmions are topologically nontrivial chiral-spin textures with a whirling configuration and hold great promise for future low-power spintronic devices including memories and logic gates.[5–8] Thus, topological structures have become an important research area in materials science and condensed-matter physics.

S. Q. Chen, Dr. S. Yuan, J. P. Zhang, T. Wang, Prof. W. W. Zhao, Prof. X. J. Liu, Prof. Z. H. Chen
School of Materials Science and Engineering
Harbin Institute of Technology
Shenzhen 518055, China
E-mail: wzhao@hit.edu.cn; zuhuang@hit.edu.cn

Prof. Z. P. Hou
Guangdong Provincial Key Laboratory of Optical Information Materials and Technology & Institute for Advanced Materials
South China Academy of Advanced Optoelectronics
South China Normal University
Guangzhou 510006, P. R. China

Prof. Z. P. Hou
National Center for International Research on Green Optoelectronics
South China Normal University
Guangzhou 510006, P. R. China

The ORCID identification number(s) for the author(s) of this article can be found under https://doi.org/10.1002/adma.202000857.

DOI: 10.1002/adma.202000857

Dr. Y. L. Tang
Shenyang National Laboratory for Materials Science
Institute of Metal Research
Chinese Academy of Sciences
Wenhua Road 72, Shenyang 110016, China

Dr. K. Li, Prof. W. W. Zhao, Prof. Z. H. Chen
Flexible Printed Electronics Technology Center
Harbin Institute of Technology
Shenzhen 518055, China

Prof. L. Chen
Department of Physics
Southern University of Science and Technology
Shenzhen 518055, China

Prof. L. W. Martin
Department of Materials Science and Engineering
University of California
Berkeley, CA 94720, USA

Prof. L. W. Martin
Materials Sciences Division
Lawrence Berkeley National Laboratory
Berkeley, CA 94720, USA

On the other hand, ferroic materials, such as ferroelectric, magnetic, and multiferroic materials, have received considerable interest in view of their field switchable spontaneous polar/magnetic ordering and wide range of practical applications including memories, sensors, and actuators.[9,10] Most of these applications require the ability to produce highly controlled thin-film versions of materials. Ferroic thin films have a tendency to form domains, areas that differ in the orientation of the order parameter and are separated by domain walls, to reduce uncompensated depolarization/demagnetization fields at the surfaces, accommodate elastic strain, and, ultimately, lower the total free energy.[11,12] Domain walls (**Figure 1**a), as one type of topological defects, have recently been shown to exhibit unexpected functionalities that differ from the bulk domains.[13–18] Therefore, although uniform domains with aligned polarization/magnetization are most common in ferroic thin films, there is both fundamental and technological interest in designing more exotic, smoothly varying dipole topologies in both ferroelectrics and magnetic materials. By delicately engineering the boundary conditions and/or size and dimensionality, more intriguing topological nanoscale spin/polar textures, such as flux-closure domains, vortices, bubbles, skyrmions, and merons have been revealed in ferroic materials (Figure 1b–g).[19–22] For the 2D systems, these complex topological structures are generally characterized by the topological number/charge N,[5,6,23,24] which can be calculated via the closed-loop integral of the vector field angle, i.e.

$$N = \frac{1}{4\pi}\int \mathbf{n}\left(\frac{\partial \mathbf{n}}{\partial \mathbf{x}} \times \frac{\partial \mathbf{n}}{\partial \mathbf{y}}\right) \mathrm{d}x\,\mathrm{d}y \tag{1}$$

where $\mathbf{n}$ is the direction vector of order parameter (magnetization or polarization).[24]

Topological structures in magnetic materials have been studied extensively and the interplay between the topological structures and the spins of conduction electrons can lead to many fascinating topological properties (e.g., topological Hall effect) and potential spintronic applications.[24] Dating back to the late 1940s, Kittel proposed that different spin texture in magnetic materials could be possible depending on the relative strength of exchange, anisotropy, and magnetostatic energies.[25] Flux-closure domains and vortices have similar structures and common in magnetic materials, especially when they are reduced to the nanoscale.[26–28] Note that both of them are due to the magnetostatic effect. Magnetic bubbles were also studied extensively since their first observation in 1960s in ferromagnetic films with strong perpendicular anisotropy,[29] and were applied to memory devices soon after.[30] Note that there are two types of bubbles in ferromagnetic materials, wherein soft-type bubbles have a closed domain wall and hard-type bubbles have an unclosed domain wall.[31] Another important topological spin structure are magnetic skyrmions.[5,7,8,24] There are two major types of magnetic skyrmions, i.e., Bloch- (or spiral-type) and Néel-type (or hedgehog-type), both of them have topological charges of $N = 1$.[7] Although magnetic skyrmions were predicted more than two decades ago,[32] the first experimental observation of magnetic skyrmion can be traced back to just 2009 in chiral magnets.[33] Since then, magnetic skyrmions have been observed in various material systems (including ferromagnets, ferrimagnets, and antiferromagnets) and have become one of the hottest topics in condensed matter physics.[34–41] This is mainly because skyrmions are energetically stable on the nanometer scale and exhibit energy-efficient, current-driven behavior that is suitable for next-generation low-power spintronic devices.[42] In addition to the discovery of skyrmions, other new forms of topological spin textures have been studied in magnetic materials.[43–46] One particularly interesting structure is the so-called meron, wherein

Shanquan Chen received his M.Sc. degree in materials science and engineering from Shenzhen University in 2018. He is now a Ph.D. student in the School of Materials Science and Engineering at Harbin Institute of Technology, Shenzhen. He joined Prof. Zuhuang Chen's group in early 2019. His current research interests mainly focus on epitaxial thin-films growth and emergent phenomena at ferroic oxide thin films and heterostructures.

Shuai Yuan received his B.Eng. degree in theoretical and applied mechanics in 2009 and his Ph.D. degree in engineering mechanics in 2018 from Sun Yat-sen University in China. Since 2019, he has been working in Prof. Zuhuang Chen's Group as a postdoctoral researcher at Harbin Institute of Technology. His research interests involve physics and mechanics of topological structures in ferroelectric, ferromagnetic, and multiferroic materials.

Zuhuang Chen received his Ph.D. degree in materials science from Nanyang Technological University. He then worked as a postdoc researcher at the University of Illinois at Urbana-Champaign and University of California at Berkeley under the supervision of Prof. Lane Martin and Prof. R. Ramesh. He joined Harbin Institute of Technology in 2018 as a faculty professor and is currently leading a research group focusing on ferroelectric thin films, multiferroic heterostructures, and strongly correlated oxides.

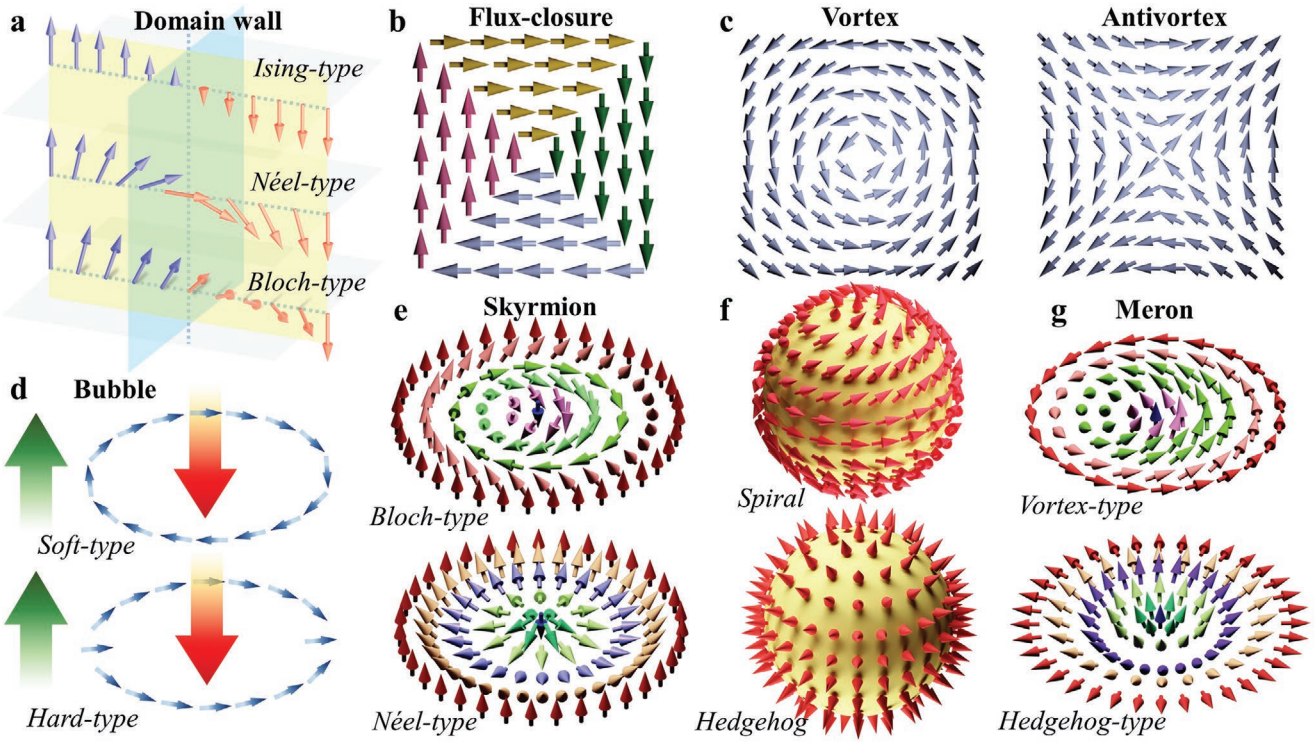

Figure 1. Schematics of typical topological structures in ferroics. Order parameter, such as polarization and magnetization represented as arrows. a) Different types of domain walls; note that ferroelectric domain walls were assumed to be predominantly Ising-type, while domain walls in magnetic materials are typically of Bloch-type (the magnetization vector rotates continuously in a plane parallel to the wall plane) or Néel-type (the magnetization vector rotates in a plane normal to the wall plane); b) flux-closure; c) vortex and antivortex; d) bubble, including soft-type and hard-type; e) Bloch-type and Néel-type skyrmion; f) spiral and hedgehog skyrmion ball; g) meron, including vortex-type and hedgehog-type. Note that skyrmion corresponds to 2D projection from an original 3D skyrmion ball, and meron can be considered as one-half skyrmion.

the spin at the core points in the up or down direction but those at the periphery align in the plane; thus a meron is topologically equal to one-half of a skyrmion with $N = 0.5$.[44,47–49]

Inspired by the observation of various topological spin textures in magnetic materials, considerable interest has also been given to the exploration of polar topologies in ferroelectrics. Both theoretical and experimental studies of topological structures in ferroelectrics appeared much later than their magnetic counterparts; mainly because they were considered difficult to realize since there is a strong lattice-polarization coupling in bulk ferroelectrics which should impose a significant energy cost for rotating the polarization away from the symmetry-allowed directions. In the early 2000s, however, Fu and Bellaiche et al. first reported the realization of vortex pattern in ferroelectric $BaTiO_3$ quantum dots and wires using a first-principles-derived effective-Hamiltonian approach.[50] Different from in bulk materials, the depolarization field increased dramatically and the magnitude of the polarization was suppressed in low-dimensional ferroelectrics, resulting in weak anisotropy. Therefore, the electric dipoles in the nanostructured ferroelectrics could rotate and be redistributed head-to-tail to form a flux-closure domain or vortex-domain structure in order to reduce the depolarization energy.[50–52] Since that time, additional theoretical investigations have predicted ferroelectric vortices and flux-closure domain patterns in ferroelectric epitaxial ultrathin films,[51] nanodisks and nanorods,[52] nanodots,[53] nanoparticles,[54,55] nanotubes,[56] nanowires,[57] etc. In contrast, there are fewer experimental observations, mainly due to challenges in realizing such nanostructured ferroelectrics, as well as a lack of adequate characterization tools. In 2008, Gruveman et al. made one of the earliest claims of the experimental observation of vortex-domain structures during polarization switching in $PbZr_{0.2}Ti_{0.8}O_3$ (PZT) epitaxial thin films by piezoelectric force microscopy.[58] Direct evidence for the formation of rotating polarization at atomic scale was made in 2011 when experimentalists were able to directly observe continuous polarization rotation near the interfaces of ferroelectric thin films using aberration-corrected (scanning) transmission electron microscopy (TEM).[59,60] Since then, several exotic polar topologies such as flux-closure domains,[61–65] vortices,[66–71] non-Ising-like domain walls,[72–74] center-type domains,[68,70,75,76] labyrinthine domains,[77] bubbles,[78] incommensurate curl domains,[79] spiral states,[80] hedgehog states,[81] and polar skyrmions,[82,83] have been revealed in various ferroelectric materials. Which kind of polar topology develops would depend on the relative magnitudes of various energies, such as elastic (i.e., strain), electrostatic (i.e., depolarization), polarization/chemical gradient, and interfacial coupling energies. Recent advances in layer-by-layer epitaxial growth provide a great opportunity to engineer different energies and phase competitions in ferroelectric thin films and heterostructures.[84–86] For instance, in superlattices of $(PbTiO_3)_n/(SrTiO_3)_n$ with n = 1–2 unit cells, improper

ferroelectricity emerges because of antiferrodistortive/ferroelectric coupling at the interfaces.[84] At relatively large length scales ($n > 20$), these superlattices form flux-closure domain patterns in order to reduce depolarization fields,[59,63] while nonuniform polarization modes consisting of highly ordered vortex/skyrmion phase are stabilized in $(PbTiO_3)_n/(SrTiO_3)_n$ superlattices with n = 10–20 under different epitaxial strains.[69,83] Although the nontrivial topologies in ferroelectrics are analogous to the spin topologies, the fundamental physical origin is completely different. The spin topologies, such as magnetic skyrmions, mostly originate from the competition of exchange interaction, magnetic anisotropy, dipole–dipole interaction (i.e., magnetostatic interaction), and/or the chiral Dzyaloshinski–Moriya interaction (DMI).[87] In ferroelectrics, there is no such magnetic interactions. The elastic, electrostatic, and gradient energies compete such a way that topological nontrivial polar texture could occur automatically in ferroelectric system. The presence of nonuniform polarization mode in ferroelectrics enables the possibility to create novel functionalities previously inaccessible in the parent materials, such as enhanced electronic conductivity,[14,88] enhanced magnetization,[16] giant electromechanical response,[78] chirality,[89,90] negative capacitance,[91,92] etc., and could provide a new paradigm for potential applications in nanoelectronic devices, including ultradense nonvolatile memories and low-power transistors.

This progress report aims to give a timely review on the advance and breakthrough over the past decade in topological structures in ferroic thin films and heterostructures. As a starting point, we focus on magnetic skyrmions in metallic thin films and heterostructures, and topological Hall effect (THE) in magnetic oxide thin films and heterostructures. We then introduce typical polar topologies, such as domain walls, flux-closure domains, vortices, bubble domains, polar skyrmions, and associated functionalities recently observed in ferroelectric epitaxial thin films and heterostructures. Finally, we conclude this review with an outlook for this burgeoning field.

2. Topological Structures in Magnetic Thin Films and Heterostructures

2.1. Skyrmions in Magnetic Metallic Thin Films and Heterostructures

In the field of magnetism, the concept of topology is introduced to explain the physical behaviors of some exotic spin configurations, including vortices,[93] merons,[44] bubbles,[25] skyrmions,[5,8] bobbers,[94] and hopfions,[27] where the physical behaviors of these magnetic states are significantly affected by their topological characteristics. For the stabilization of magnetic structures, the Heisenberg exchange energy plays a dominate role and generally favors adjacent spins to orientate along the parallel or antiparallel orientation. The topological spin structures, however, belong to the noncollinear spin configurations. Thus, some other energy terms that can stabilize the noncollinear textures should be introduced. In general, the noncollinear spin textures can be stabilized by magnetostatic interaction (i.e., dipole–dipole interaction),[95] DMI,[96,97] four-spin exchange interaction,[37] and frustrated exchange interaction.[98,99] In the past decade, most investigations are focused on the DMI because its generation is closely connected with the interface engineering in the field of modern thin-film fabrication technique. DMI belongs to a kind of asymmetric exchange interaction that originates from the combination of spin–orbit coupling and inversion symmetry breaking. Its Hamiltonian can be written as[100]

$$H_{\mathrm{DMI}} = -\sum_{ij} \mathbf{D}_{ij} \cdot \mathbf{S}_i \times \mathbf{S}_j \tag{2}$$

where $\mathbf{S}_i$ is the ith spin vector and $\mathbf{D}_{ij}$ is the DMI vector. The DMI favors a canting of the two neighboring spins and supports a rotating magnetization alignment tending to an angle with a fixed rotation manner (that is so called "chirality"). Depending on the type of inversion symmetry breaking, there are two types of DMI, namely, the bulk DMI and interfacial DMI. The bulk DMI originates from intrinsic noncentrosymmetric lattice structures typically observed in B20 crystals, such as MnSi and FeGe.[35,36,38,101] While the interfacial DMI generally exists in magnetic multilayered ultrathin films (**Figure 2**a), where the inversion symmetry is naturally broken at the interface/surface.[102,103] Note that the strength of DMI is proportional to the spin–orbit coupling, whose magnitude increases with the atomic number. Therefore, a large DMI is typically found in materials with heavy element (e.g., Pt and Ir), which exhibit strong spin–orbit coupling strength.

Among the numerous DMI-stabilized topological spin configurations, magnetic skyrmions have received the most attention in view of their intriguing electromagnetic properties,[5,8,40,94,104–113] such as THE,[112,114] and ultralow threshold for current-driven motion.[110,111] These novel magnetoelectronic properties, in combination with their fixed chirality, nanoscale size, and stable particle-like features, make magnetic skyrmions the most promising candidates for carrying information in future magnetic memories or logic circuits.[5,7,8,24,115] In the following, we will mainly review the development of the skyrmions in ferromagnetic thin films and heterostructures driven by interfacial DMI.

The concept of skyrmion was initially proposed by Skyrme in the 1960s in the field of particle physics.[116] In the field of magnetism, skyrmions was first proposed by Bogdanov and Yablonskiĭ in 1989.[117] Subsequently, in 1994, Bogdanov and Hubert predicted that magnetic skyrmions may exist in noncentrosymmetric magnetic crystals with a bulk DMI.[118] In 2001, Bogdanov and Rößler further predicted that the magnetic skyrmions could also exist in the asymmetric magnetic films or multilayers with interfacial DMI.[119] Until 2009, Mühlbauer et al. first experimentally verified the existence of skyrmions in the chiral magnet MnSi at 29 K by using neutron scattering technique.[33] Meanwhile they found that skyrmions were densely arranged into hexagonal lattices that are also called "skyrmion lattice." Then, in 2010, Yu et al. directly observed the skyrmion lattice in real space in the $Fe_{0.5}Co_{0.5}Si$ thin plate at 25 K by using the Lorentz transmission electron microscopy (LTEM).[36] Based on neutron scattering and LTEM techniques, researchers further reported the existence of skyrmions in various bulk chiral magnets, such as FeGe,[36,120] Cu_2OSeO_3,[38] and Co–Zn–Mn.[101]

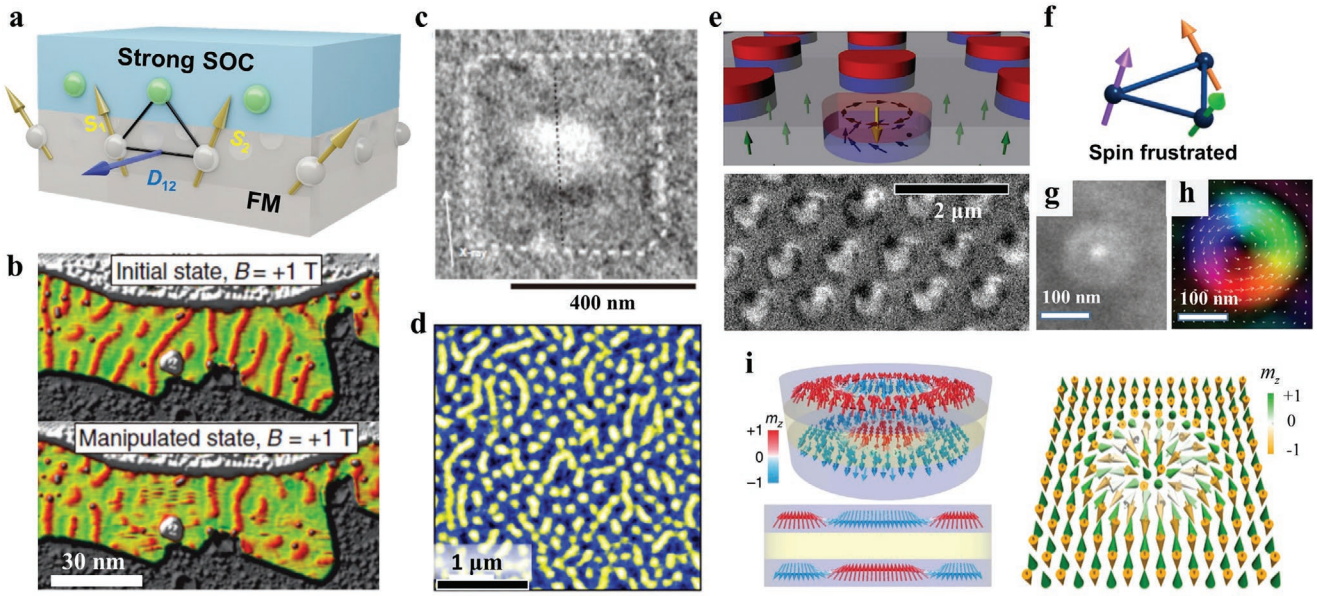

Figure 2. Skyrmions in metallic magnetic thin films and heterostructures. a) Schematics of interfacial Dzyaloshinskii–Moriya interaction (DMI) in multilayer heterostructure. The top layer is a heavy metal with strong spin–orbit coupling and the bottom is ferromagnetic layer. S_1 and S_2 label the spins of neighboring atoms, and D_{12} is the corresponding Dzyaloshinskii–Moriya vector. The exchanged-coupled neighboring parallel moments S_1 and S_2 tend to tilt due to the competition interaction in the heterostructure. b) Manipulation of the magnetic states of the PdFe bilayer at $T = 4.2$ K under electrical filed of 0.1 V (spin spiral state, top) and 1 V (skyrmions, bottom). b) Reproduced with permission.[121] Copyright 2013, American Association for the Advancement of Science. c) X-ray magnetic circular dichroism photoemission electron microscopy image of a Néel-type skyrmion observed at room temperature and zero external magnetic field in sputtered ultrathin Pt/Co/MgO nanostructures. Reproduced with permission.[123] Copyright 2016, Springer Nature. d) MFM image in the skyrmion state for the Pt/Co/Fe/Ir multilayer. Reproduced with permission.[124] Copyright 2017, Springer Nature. e) A schematic (top) and MFM image (bottom) of the artificial skyrmions observed in hybrid structures of Co nanodots on a Co/Pd underlayer with perpendicular magnetic anisotropy. Reproduced under the terms of the CC-BY Creative Commons Attribution 4.0 International License (https://creativecommons.org/licenses/by/4.0).[128] Copyright 2015, Springer Nature. f) Schematic of spin frustration. g) LTEM image of frustrated skyrmions observed in a frustrated kagome Fe_3Sn_2 magnet. h) Spin texture of the frustrated skyrmion in (g). f–h) Reproduced with permission.[129] Copyright 2017, Wiley-VCH. i) Schematics of antiferromagnetic skyrmions (right) and synthetic antiferromagnetic skyrmions (left). Left: Reproduced under the terms of the CC-BY Creative Commons Attribution 4.0 International License (https://creativecommons.org/licenses/by/4.0).[132] Copyright 2016, Springer Nature. Right: Reproduced under the terms of the CC-BY Creative Commons Attribution 4.0 International License (https://creativecommons.org/licenses/by/4.0).[135] Copyright 2016, Springer Nature.

The investigations of skyrmions in ferromagnetic thin films and heterostructures are later than that of the bulk. In 2011, Heinze et al. first reported the existence of skyrmions in the magnetic ultrathin films, i.e., Fe monolayer grown on Ir substrate, by using spin-polarized scanning tunneling microscopy (SP-STM) at 11 K.[37] By further using a local spin-polarized current from a STM tip, Romming et al. realized both a controllable writing and deleting of Néel-type skyrmions with sub-5 nm feature size in a PdFe bilayer on the (111)-orientated substrates at 4.2 K (Figure 2b).[121] In 2015, Jiang et al. first reported the room-temperature stabilized skyrmion bubbles with a diameter of ≈1 μm in the Ta(5 nm)/CoFeB(1.1 nm)/TaO_x (3 nm) multilayered ferromagnetic ultrathin films grown by using the magnetron sputtering.[40] Meanwhile, they also realized a generation and motion of skyrmions in the geometrical constrictions by using a spin-polarized current. Their work has motivated researchers to explore the stable, nanosized skyrmions at room temperature in the multilayered ferromagnetic ultrathin films. One year later, Moreau-Luchaire et al. reported the sub-100 nm skyrmions at room temperature in the Ir/Co/Pt asymmetric multilayers by using a magnetization-sensitive scanning X-ray transmission microscopy (STXM) technique.[122] In the same year, using the X-ray magnetic circular dichroism photoemission electron microscopy (XMCD-PEEM), Boulle et al. also reported the observations of stable skyrmions in Pt/Co/MgO ultrathin films at room temperature (Figure 2c).[123] More intriguingly, they fabricated the films into geometrical constrains and zero external magnetic field stabilization were further realized due to the strongly pinning effect from the geometrical edge. Subsequently, Woo et al. not only reported the observation of room-temperature stabilized skyrmions in the [Pt(3 nm)/Co(0.9 nm)/Ta(4 nm)]$_{15}$ and [Pt(4.5 nm)/CoFeB(0.7 nm)/MgO(1.4 nm)]$_{15}$ multilayer stacks, but also realize a current-induced motion of skyrmions in a geometrically confined nanodisk.[102] In 2017, Soumyanarayanan et al. reported a room-temperature sub-50 nm skyrmions in the tunable Ir/Fe/Co/Pt multilayer stacks (Figure 2d),[124] which demonstrated that the magnetic interactions for the stabilization of skyrmions can be tuned by varying the compositions of ferromagnetic films. In 2019, Wang et al. obtained the ultrahigh-density sub-100 nm skyrmions in the [Pt/Co/Ta]$_n$ multilayer stacks by tuning the magnetic anisotropy and DMI. Meanwhile, they found that the film with in-plane magnetic anisotropy possess a larger skyrmion density than that of the film with perpendicular magnetic anisotropy.[125]

In addition to the asymmetric ferromagnetic ultrathin films with interfacial DMI, researchers also found that the room-temperature

skyrmions can also be stabilized in the films without DMI, such as the artificial skyrmions,[126–128] and frustrated skyrmions.[129] In 2013, Sun et al. theoretically proposed that the so-called "artificial skyrmions" can be created by embedding a magnetic vortex into a perpendicularly magnetized film.[126] These topological spin configurations possess a similar spin texture with that of Bloch-type skyrmions. Moreover, the artificial skyrmions are proposed to be able to keep stable at room temperature and even under zero magnetic field. Soon after, the artificial method for creating skyrmions have been experimentally confirmed.[127,128] For instance, in 2015, Gilbert et al.[128] realized such an artificial skyrmion at room temperature in Co/Pd multilayered films (Figure 2e). Skyrmions can also exist in geometrically frustrated magnets with competing exchange interactions.[98,99] Theoretical works has predicted that the frustrated skyrmions may exhibit intriguing magneto-electrical properties, such as the multiple topologies and unfixed helicity.[98,99] In 2017, Hou et al first experimentally observed skyrmionic magnetic bubbles at room temperature in a frustrated Fe_3Sn_2 magnet with Kagome lattice by using LTEM (Figure 2f–h).[129,130] In 2019, Kurumaji et al. demonstrated a Bloch-type skyrmion state in a frustrated centrosymmetric triangular-lattice magnet Gd_2PdSi_3. Meanwhile, the authors also observed a giant topological Hall response.[131] However, all the skyrmions in the frustrated magnets are observed in the bulk form at current stage. Hence, searching for frustrated skyrmions in thin film form will be a hot topic for the further development of skyrmions.

In the past decade, the investigations on skyrmions are mainly focused on ferromagnetic systems. Very recently, researchers found that the antiferromagnets could host skyrmions also.[46,132–135] In contrast to the ferromagnetic skyrmions, the antiferromagentic skyrmions possess a zero topological charge ($N = 0$) because they can be considered as two skyrmions coupled with opposite topological number (Figure 2i). Such a special spin texture endows them several intrinsic merits for their practical applications in the field of spintronics. For example, when ferromagnetic skyrmions are driven by the spin current, a transverse shift, namely skyrmion Hall effect (SkHE),[113,136] usually accompanies with the longitudinal motion. The SkHE originates from the Magnus force induced by the topological spin structure of the skyrmions and may lead to the destruction of skyrmions at the edge of the samples.[134,135] However, the Magnus force during the current-induced motion of antiferromagnetic skyrmions can be canceled due to their zero topological charge and hence the antiferromagnetic skyrmions can move straightly along the direction that the current is injected.[106,132,134,137] Moreover, their motion speed is also significantly enhanced in contrast to that of ferromagnetic skyrmions.[134,135] Despite their great potentials, the materials hosting the antiferromagnetic skyrmions are not reported yet. Very recently, the synthetic antiferromagnetic skyrmions are experimentally reported in the magnetic thin films (Figure 2i, left).[132] Until 2019, Legrand et al. first experimentally observed the antiferromagentic skyrmions in the synthetic antiferromagnets Pt/Co/Ru multilayered film at room temperature.[46] Subsequently, Dohi et al. realized the current-induced motion of antiferromagnetic skyrmions at room temperature.[133] Meanwhile, their work experimentally confirmed that theoretical expectations on the antiferromagnetic skyrmions, including high motion speed and negligible SkHE, which greatly promotes the practical application of antiferromagnetic skyrmions in the field of spintronics.[106,132,138,139] Due to the intriguing properties, searching for new material systems hosting antiferromagnetic skyrmions and investigating the correlated dynamics have become one of the most promising directions for the further development of skyrmions.

Skyrmions are widely considered as promising candidates for carrying information in future high-dense, low-power and high-speed magnetic memories and logic circuits (**Figure 3**a).[109,140] As the information bits, magnetic skyrmions are required to be controllably written, deleted, and read through a purely electrical manner for easy integration into modern electronic technology.[110] To date, electrical writing and deletion of skyrmions have been generally realized via the use of the spin-polarized

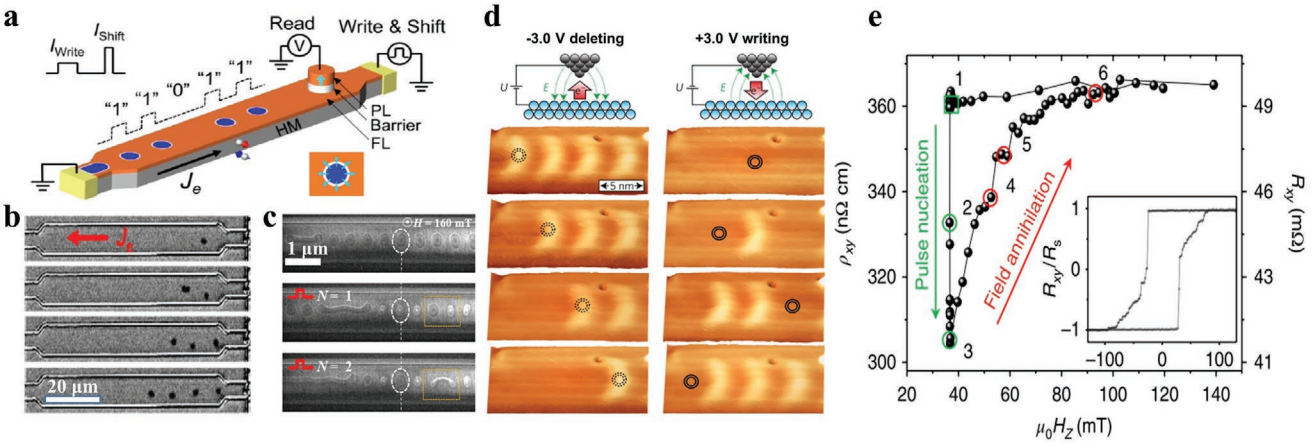

Figure 3. Writing, deleting, and reading of skyrmions. a) Schematic of a skyrmion-based race-track memory device. b) Generation of skyrmions in a skyrmion-based race-track memory device by using a series of write pulses and shift pulse. a,b) Reproduced with permission.[140] Copyright 2016, American Chemical Society. c) Current-induced helicity switching of frustrated skyrmions. Reproduced with permission.[142] Copyright 2019, Wiley-VCH. d) Perspective views of electrical-field-induced writing and deleting of individual magnetic skyrmions in an Fe triple layer subsequently by using SP-STM. Reproduced with permission.[143] Copyright 2017, Springer Nature. e) Variation of Hall resistance (ρ_{xy}) with the skyrmion nucleation process. Reproduced with permission.[107] Copyright 2018, Springer Nature.

current on basis of the spin-transfer torque or spin–orbit torque effect (Figure 3b).[140] Initially, Jonietz et al. and Schulz et al. experimentally reported a low threshold current density of 10^6 A/m^2 for de-pinning motion of skyrmions in the chiral bulk crystals,[110,111] and such a current density is 4–5 orders of magnitude lower than that required for the de-pinning motion of ferromagnetic domain walls.[141] However, further investigations showed that such a low current density just corresponds to a low motion speed and the speed increases with the increase of the current density.[106,110] At current stage, the current for the creation, deletion, and motion with a relatively high speed of skyrmions require a high current density ranging from 10^9–10^{12} A m^{-2}.[40,102,103,106,109] Recently, Hou et al., experimentally realized a current-driven helicity switching of Bloch-type frustrated skyrmions at room temperature (Figure 3c), which opens a new direction for spintronic device designs, e.g., the skyrmion-based multistate memories.[142]

The large driven current density leads to the large energy consumption, and meanwhile the Joule heating originating from the inject current is detrimental to the stability of skyrmion bits. In contrast, the electric-field method provides a potentially effective route to achieve the low-energy-dissipation and low-Joule-heating target, as the operations generate almost no current (Figure 3d).[143–145] Moreover, the electric-field approach could avoid the unexpected displacement of skyrmions during the writing process. These features are of great significance to practical applications and have thus promoted the usage of electric field instead of current to manipulate skyrmions. In addition to the electric-field-method, the strain and laser are also applied to manipulate the skyrmions with an expectation of low-energy consumption.[146,147]

Since the applications of skyrmions in the spintronic devices require identifying the behaviors and locations of skyrmions, the reading of skyrmions is also an important task for practical applications. At current stage, numerous state-of-art microscopy magnetic imaging techniques, including magnetooptical Kerr microscopy (MOKE),[40] LTEM,[36,101] magnetic force microscopy (MFM),[124] SP-STM,[37] SXTM,[122] and X-ray magnetic circular dichroism (XMCD),[123] are applied. Although these technologies are efficient for the detection of skyrmions, the electrical reading is an essential step toward the applications of skyrmion-based information devices. One promising method to electrically read skyrmions is on basis of the THE, which will be discussed in detail next section (Figure 3e).[107] Another method to read skyrmions is based on the large on/off ratio of skyrmions by integrating the skyrmion-hosting films into the magnetic tunnel junction (MTJ) sensors.[148,149] The magnetoresistance of MTJ is sensitive to the variation of the magnetic environment and hence the creation and annihilation of skyrmions can be electrically detected.

For the last decade, we have witnessed the booming development of skyrmions, in view of their fascinating physics and promising applications in the field of low-power, high-speed spintronic devices. In this section, we have reviewed the recent progress of skyrmion-electronics from the point view of both skyrmion-hosting materials and possible practical applications. However, we should note that other topological spin textures, such as magnetic vortices, merons, bobbers, magnetic bubbles, also exhibit numerous intriguing topological properties that are of great significance to the further development of spintronics. These topological spin configurations together with magnetic skyrmions have constructed a large family of magnetic topologies, and the relevant investigations has led to the emerging a brand-new field of "topological magnetism". In the coming decade, the investigations of topological magnetism will continue to be active in the field of materials science and condensed matter physics.

2.2. Topological Hall Effect in Magnetic Oxide Thin Films and Heterostructure

Besides the magnetic skyrmions observed in magnetic metals or intermetallic compound,[124,150–153] there have been several reports very recently on the magnetic skyrmions in a variety of magnetic oxide epitaxial thin films and heterostructures, where a subtle interplay between spin, charge, orbital and lattice degrees of freedom across heterointerfaces is responsible for the phenomena.[34,41,150,154–158] However, direct real-space observation of skyrmions in functional oxide thin films and heterostructures is experimentally challenging primarily because of the low Curie temperature and/or weak magnetization moment in the oxide systems. Alternatively, an indirect transport-measurement method, i.e., topological Hall measurement, has been used to detect the skyrmion state in ferromagnet and antiferromagnet.[114,152,159–162] The THE originates from scalar spin chirality $\left[\chi_{ijk} = \vec{\mathbf{S}}_i \cdot \left(\vec{\mathbf{S}}_j \times \vec{\mathbf{S}}_k\right)\right]$ concomitant with noncoplanar spin configurations. When electrons pass through a skyrmion, the spin of the conduction electron will experience an emergent magnetic field (Berry curvature) through interaction with skyrmions, which deflects the electrons perpendicular to the current direction.[163] Therefore, it will cause an additional contribution to the observed Hall signal that is termed as THE. The Hall resistivity can be expressed by

$$\rho_{\mathrm{H}} = \rho_{\mathrm{OHE}} + \rho_{\mathrm{AHE}} + \rho_{\mathrm{THE}} \tag{3}$$

where the first, second, and third terms denote the ordinary, anomalous and topological Hall resistivities, respectively. The topological Hall resistivity ρ_{THE} originates from the real-space Berry phase and is proportional to the skyrmion density.[114,152,159,160,164,165] THE has a distinct hump-like feature in Hall resistivity near the coercive field,[34,154] and can be quantitatively extracted from the total Hall resistivity measurement by subtracting off the ordinary and anomalous Hall resistivities. Therefore, THE is considered as a hallmark of skyrmions and thus has been used to detect the presence of magnetic skyrmion.[34,114,152,154,156,157,159,160]

Recently, THE and possible magnetic skyrmions have been reported in a variety of ferroic oxide epitaxial thin films and heterostructures.[34,41,154,156,157,166–170] Most of the research has focused on $SrRuO_3$ epitaxial thin films and heterostructures since $SrRuO_3$ exhibits ferromagnetism and also large intrinsic spin–orbit coupling, providing the basic ingredients for DMI and skyrmion formation.[34,41,154,156,157] The THE is attributed to the interfacial DMI induced by the strong spin–orbit coupling in 4d/5d transition metal oxides (e.g., ruthenates and iridates) and broken inversion symmetry at the heterointerface/surface.

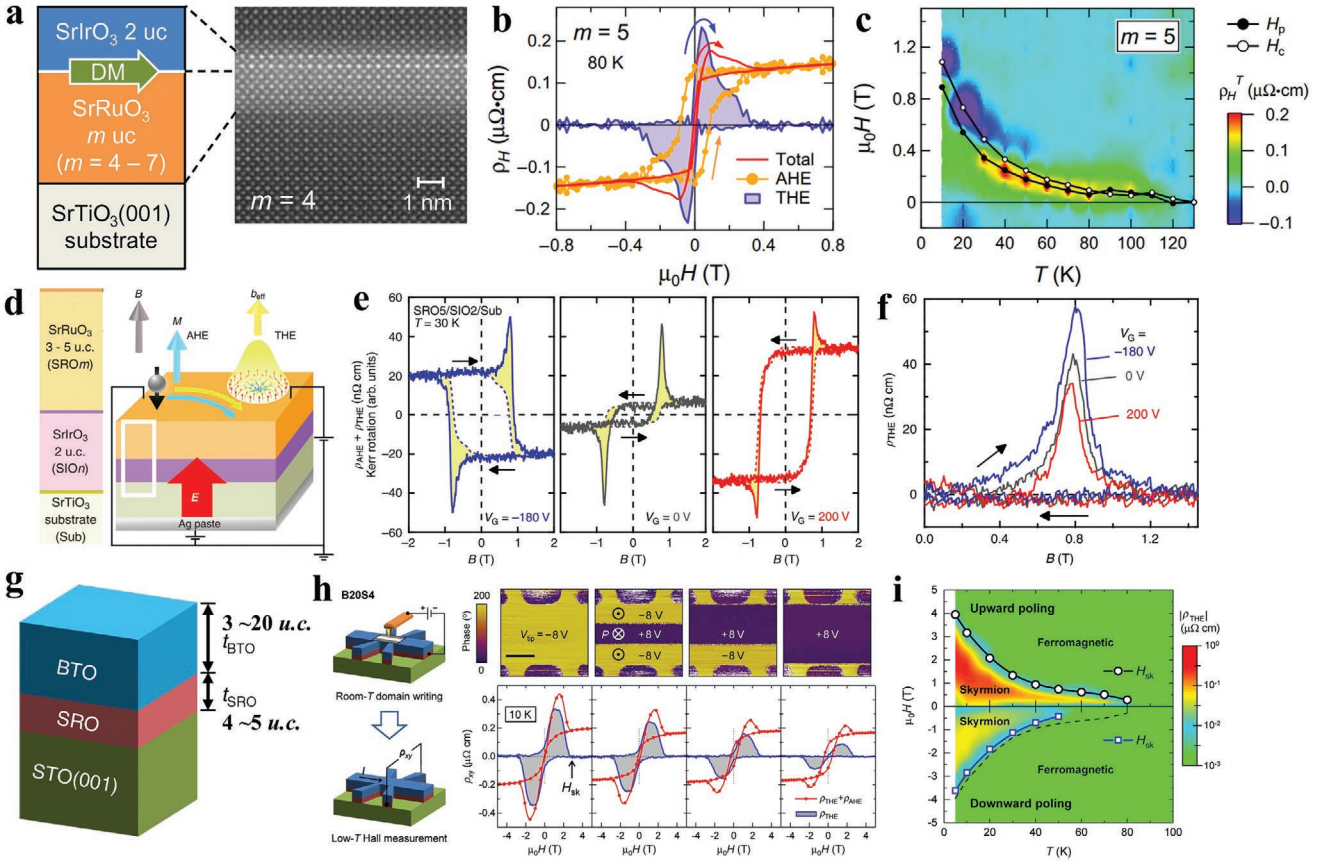

Figure 4. Topological Hall effect (THE) and related modulation in $SrRuO_3$ heterostructures. a–c) THE in the $(SrRuO_3)_m$–$(SrIrO_3)_2$ bilayers (m = 4–7). a) Schematics and HAADF-STEM image of the bilayer structure; b) contribution from AHE and THE of m = 5 at 80 K; c) color map of topological Hall resistivity in the T–H plane for m = 5. Black open and filled symbols represent coercive field (H_c) and the field at which topological Hall resistivity reaches its maximum (H_p), respectively. a–c) Reproduced with permission.[34] Copyright 2016, The Authors, published by American Association for the Advancement of Science (AAAS). Reprinted/modified from ref. [34]. © The Authors, some rights reserved; exclusive licensee American Association for the Advancement of Science. Distributed under a Creative Commons Attribution NonCommercial License 4.0 (CC BY-NC) http://creativecommons.org/licenses/by-nc/4.0/. d–f) THE in $SrRuO_3/SrIrO_3/SrTiO_3$ heterostructure under the application of a gate electric field. d) Schematics of magnetotransport properties observed in $SrRuO_3/SrIrO_3$ heterostructure under the application of gate voltage V_G. e) Hall resistivities (ρ_{AHE} + ρ_{THE}) and f) topological Hall resistivity (ρ_{THE}) of $SrRuO_3$(5 uc)/$SrIrO_3$(2 uc) bilayer films under gate voltage V_G = –180, 0, and 200 V at 30 K. d–f) Reproduced under the terms of the CC-BY Creative Commons Attribution 4.0 International License (https://creativecommons.org/licenses/by/4.0).[154] Copyright 2018, The Authors, published by Springer Nature. g–i) THE in $BaTiO_3/SrRuO_3/SrTiO_3$ heterostructure controlled by ferroelectric switching. g) Schematics of $BaTiO_3$(3–20 u.c.)/$SrRuO_3$(4–5 u.c.)/$SrTiO_3$(001) heterostructures; h) piezoresponse force microscopy (PFM) phase images (top panels), correlated Hall resistivities (ρ_{AHE} + ρ_{THE}) and topological Hall resistivity (ρ_{THE}) of the $BaTiO_3$(20 u.c.)/$SrRuO_3$(4 u.c.) bilayer film in different ferroelectric poling states. The scale bar in h corresponds to 10 μm. i) The ρ_{THE} and the skyrmion phase diagrams controlled by ferroelectric switching. g–i) Reproduced with permission.[157] Copyright 2018, Springer Nature.

In 2016, Matsuno et al. reported the first observation of THE in $SrRuO_3$, where a capping layer of 5d perovskite $SrIrO_3$ was provided to enhance the spin–orbit coupling and DMI strength (**Figure 4**a–c).[34] As is shown in Figure 4c, THE with hump-like features in Hall resistivity is clearly observed over a wide region of temperature (from 10 to 120 K) and magnetic field in epitaxial bilayers consisting of itinerant ferromagnet $SrRuO_3$ and paramagnetic $SrIrO_3$.[34] Importantly, the magnitude of THE rapidly decreases with increasing thickness of $SrRuO_3$ layer and completely disappears when $SrRuO_3$ layer thickness is above 6 uc, strongly suggesting that THE is derived from interfacial DMI. Furthermore, an interface-driven Néel-type magnetic skyrmions with feature size of ≈10 nm is proposed to exist in ultrathin layers of $SrRuO_3$. In addition, Ohuchi et al. found that the observed THE and associated skyrmion in the $SrRuO_3$/$SrIrO_3$ heterostructures can be effectively controlled by an electric field (Figure 4d–f).[154] The magnitude of ρ_{THE} get larger (smaller) when the negative (positive) gate voltage is applied. The authors further suggest that the electric-field control of THE is attributed to the change in the strength of spin–orbit coupling at the heterointerface and consequently the DMI and skyrmion density. In 2018, Wang et al. reported that THE and magnetic skyrmions with feature size of ≈50–100 nm can be created and electrically controlled at $BaTiO_3/SrRuO_3$ heterointerfaces (Figure 4g).[157] Unlike 5d perovskite $SrIrO_3$, $BaTiO_3$ is ferroelectric with negligibly weak spin–orbit coupling. It is found that the ferroelectric-driven polar distortion in the $BaTiO_3$ layer can penetrate into $SrRuO_3$ layer and induce sizeable ionic displacement at the top three $SrRuO_3$ monolayers. Such ferroelectric proximity effect at the heterointerface can

Table 1. Comparison of topological Hall resistivity, maximum temperature for the topological Hall effect, and corresponding spin structure in different materials systems.

Material system	Maximum THE [μΩ cm]	Maximum temperature [K]	Spin structure	References
$SrIrO_3/SrRuO_3$	0.2	120	Néel-type skyrmion	[34]
$BaTiO_3/SrRuO_3$	0.35	80	Néel-type skyrmion	[157]
$SrTiO_3/SrRuO_3$	0.08	132	Spin chirality fluctuation	[177]
$SrRuO_3$	0.3	80	Néel-type skyrmion	[156]
$SrRuO_3/La_{0.7}Sr_{0.3}MnO_3$	0.28	150	Noncoplanar spin structure	[182]
H_xSrRuO_3	0.03	100	Unclear	[172]
EuO	12	50	Bloch-type skyrmion	[167]
$La_{0.7}Sr_{0.3}MnO_3/SrIrO_3$	3.5	200	Probably magnetic skyrmions	[169]
$La_{0.7}Sr_{0.3}Mn_{0.95}Ru_{0.05}O_3$	0.63	200	Skyrmion bubbles	[183]
$Ca_{0.99}Ce_{0.11}MnO_3$	120	80	Magnetic bubbles	[155]
$Pt/Tm_3Fe_5O_{12}$	0.005	430	Néel-type skyrmion	[166]

break the inversion symmetry of the $SrRuO_3$ atomic structure near the $BaTiO_3/SrRuO_3$ heterointerface and induce a considerably large DMI, and thus create emergent skyrmions in the $SrRuO_3$ interfacial layer. Since the skyrmions in $SrRuO_3$ are induced by the spontaneous polarization in $BaTiO_3$ and thus the THE and skyrmion density can be readily controlled via switching the $BaTiO_3$ polarization with electric field (Figure 4h). Furthermore, the skyrmions is stable over a wide region of temperature (from 5 to 80 K) and magnetic field (–4 to 4 T) for both polarization states (Figure 4i). Recently, THE signatures were also observed by Qin et al. in $SrRuO_3$ single layers with layer thickness ranging from 3 to 6 nm and interpreted as arising from the presence of skyrmions.[156,171] The authors further proposed that the naturally broken inversion symmetry at the film surface and the spin–orbit coupling of Ru ions gives rise to sizeable DMI in $SrRuO_3$ epitaxial ultrathin films that is responsible for the observed THE.

Although several independent studies reported indications of THE and associated skyrmions in ultrathin layers of ferromagnetic $SrRuO_3$ via transport measurements,[34,41,154,156,157,171–173] while these indications are questioned by other models very recently.[174–181] For instance, both Kan et al.[174] and Wu et al.[175] pointed out that the THE due to a skyrmion phase cannot be the only origin of the observed hump-like features in Hall signal and further suggest that film inhomogeneities could be the key factor responsible for the observed THE-like signal in $SrRuO_3$. Real-space imaging with adequate resolution of the microscopic spin texture, such as LTEM, is highly desired in order to settle the debate about the presence of skyrmions in $SrRuO_3$.

THE signal was also observed in other functional oxide thin films and heterostructures, as shown in Table 1.[34,155–157,166,167,169,172,177,182,183] For instance, the magnitude of ρ_{THE} in the ferromagnet EuO thin films can reach up to 12 μΩ cm at 50 K, nearly two orders of magnitude larger than that in $SrRuO_3$.[167] Furthermore, Vistoli et al. observed a giant ρ_{THE} with magnitude up to 120 μΩ cm at 20 K in the lightly electron-doped manganites, $Ca_{0.99}Ce_{0.01}MnO_3$ films.[155] And Shao et al. recently found that the THE can persist to room temperature in a bilayer heterostructure composed of a magnetic insulator (thulium iron garnet, $Tm_3Fe_5O_{12}$) in contact with heavy-metal Pt.[166] Very recently, Cheng et al. observed a clear THE signal (the maximum $\rho_{THE} \approx 1.0$ nΩ cm) in Pt/antiferromagnetic insulator bilayers (Pt/Cr_2O_3) at temperatures near or above the T_N (307 K for bulk Cr_2O_3), indicating the emergence of nontrivial spin textures in antiferromagnetic insulator oxide films.[162] These studies demonstrate that magnetic oxide epitaxial thin films and heterostructures represent an exciting class of materials exhibiting THE originating from topologically nontrivial spin textures, which are highly tunable through doping, strain and interface engineering.

3. Topological Structures in Ferroelectric/Ferroelastic Thin Films and Heterostructures

3.1. Domain Walls in Ferroelectric/Ferroelastic Thin Films

3.1.1. Functional Domain Walls in Ferroelectric Thin Films

A ferroelectric domain wall (FEDW) is one type of naturally occurring planar topological defects. Owing to the polarization/lattice discontinuity, domain walls themselves were found recently to exhibit emergent functionalities distinct from the bulk domains; including the observation of enhanced electronic conductivity in otherwise insulating ferroelectric and multiferroic oxides,[14] enhanced magnetization in ferroelectric–antiferromagnets,[15,16] enhanced dielectric response,[184–187] enhanced piezoelectricity,[188,189] large thermal resistance,[17] and photovoltaic effect at domain walls.[18] Despite their importance, the physics underlying domain-wall function has not yet been fully understood because of the difficulty in characterizing such confined 2D walls. Recent advances in nanoscale characterization techniques, e.g., aberration-corrected (scanning) TEM,[59,190–194] combined with precise theoretical prediction,[195] have brought to light new details about the nature of domain walls.

FEDWs have long been assumed to be predominantly Ising-type. Recently, non-Ising-like ferroelectric domain walls, such as Néel-type, Bloch-type, and mixed Ising–Néel-type, have been predicted and experimentally demonstrated in a variety of ferroelectric/multiferroic materials.[72,73,86,196,197] For instance, a

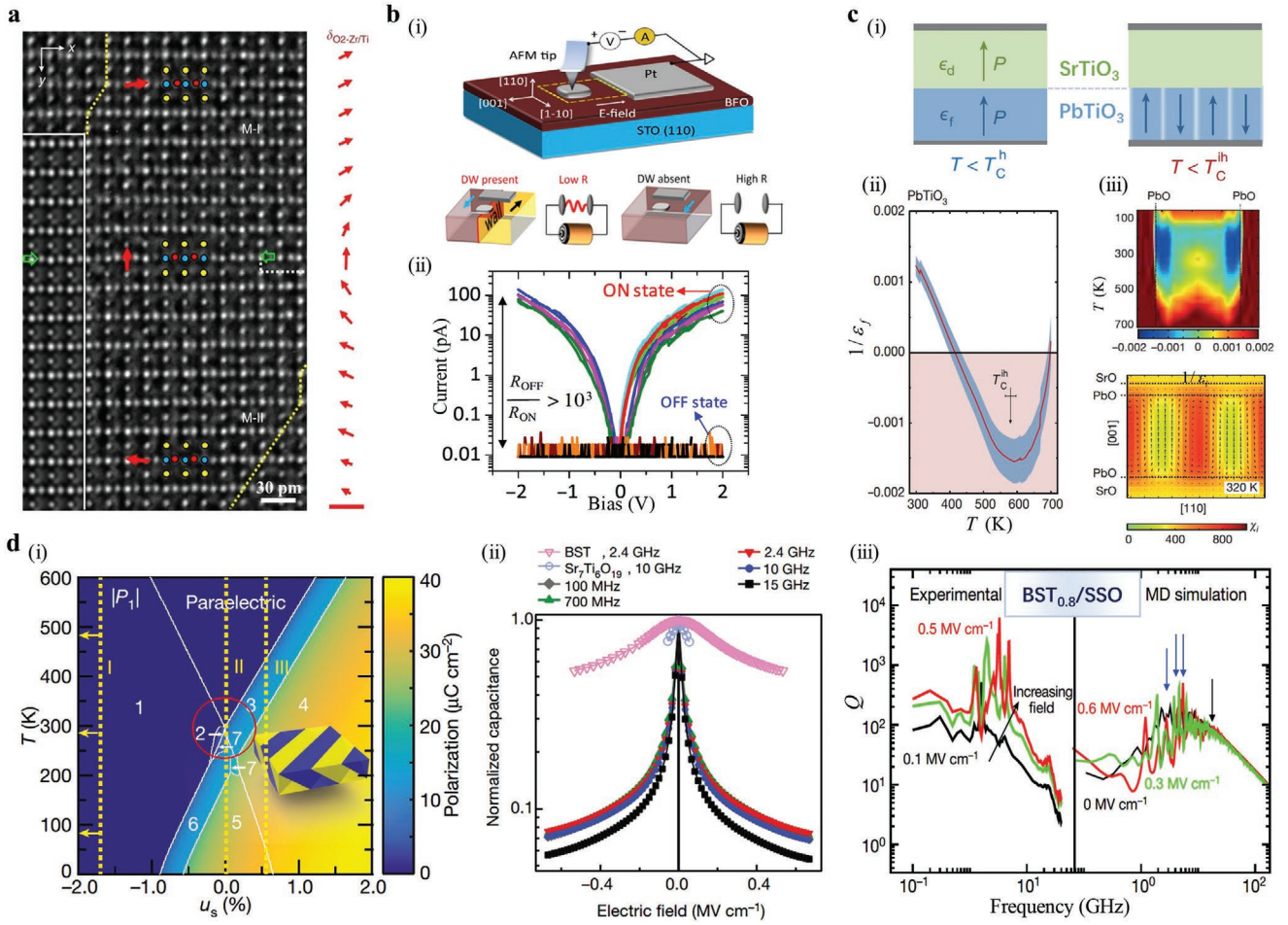

Figure 5. Examples of functional ferroelectric domain walls. a) Non-Ising domain walls in $PbZr_{0.4}Ti_{0.6}O_3$; green arrows denote the central plane of the domain wall. Reproduced with permission. Reproduced under the terms of the CC-BY Creative Commons Attribution 4.0 International License (https://creativecommons.org/licenses/by/4.0).[72] Copyright 2016, The Authors, published by Springer Nature. b) Domain wall memory and multilevel states: i) schematic of the experimental geometry and working principle of prototype ferroelectric domain wall memory device; ii) Current–bias curves of the device for the OFF and ON states. b) Reproduced with permission.[206] Copyright 2017, The Authors, published by American Association for the Advancement of Science (AAAS). Reprinted/modified from ref. [206]. © The Authors, some rights reserved; exclusive licensee American Association for the Advancement of Science. Distributed under a Creative Commons Attribution NonCommercial License 4.0 (CC BY-NC) http://creativecommons.org/licenses/by-nc/4.0/. c) Negative capacitance in ($PbTiO_3$/$SrTiO_3$) superlattices: i) schematic of the ferroelectric-dielectric ($PbTiO_3$/$SrTiO_3$) bilayer capacitor with (left) and without (right) multidomains; ii) temperature dependence of reciprocal dielectric constant of the $PbTiO_3$ layers in $PbTiO_3$/$SrTiO_3$ superlattices; iii) results of Monte Carlo simulations of a first-principles-based model for the superlattice. The top is temperature dependence of the local dielectric response resolved along the stacking direction, and the bottom is local susceptibility map at 320 K. c) Reproduced with permission.[91] Copyright 2016, Springer Nature. d) Wide microwave tunability and ultralow loss in strained $Ba_{0.8}Sr_{0.2}TiO_3$ ferroelectric thin films enhanced by resonant domain walls: i) phase diagram of $Ba_{0.8}Sr_{0.2}TiO_3$ thin film with respect to temperature T and stress u_s; ii) measured normalized capacitance which can reflect the capacitance tunability n at different frequencies for the sample ($Ba_{0.8}Sr_{0.2}TiO_3$/$SmScO_3$(110)), compared with those of epitaxial paraelectric $Ba_{0.71}Sr_{0.29}TiO_3$ (BST) and $Sr_7Ti_6O_{19}$ films; iii) experimental quality factor Q (left) and Q_y obtained by molecular dynamics (MD) simulations (right) for the aa_1/aa_2 domain structure in the sample. d) Reproduced with permission.[215] Copyright 2018, Springer Nature.

Néel-like domain wall imaged by atom-resolved TEM has been revealed in a $PbZr_{0.4}Ti_{0.6}O_3$ crystal (**Figure 5**a). As is shown, a continuous rotation of polarization (i.e., oxygen displacement relative to Zr/Ti) across the FEDW forms a structure similar to that of a Néel wall in ferromagnets. Mixed Ising–Néel-type domain walls have been revealed in PZT and $BiFeO_3$ (BFO) epitaxial thin films by using scanning transmission electron microscopy (STEM) and second-harmonic generation microscopy.[60,73,74] Unlike Ising-type walls, the mixed character will have a nonzero polarization component at the wall center, thus resulting in a electrostatic potential step at the domain wall, thereby inducing accumulation of free carriers and/or mobile charged defects into the wall plane, which may promote the enhancement of electronic conductivity.

One of the most interesting features of FEDWs is their conductivity. To date, conductivity at domain walls has been identified in a range of ferroelectric/multiferroic materials (including BFO,[88,198] $LiNbO_3$,[199] $BaTiO_3$,[200] $ErMnO_3$,[201] PZT,[202] etc.), while the exact mechanism of the domain-wall conductivity remains under debate. In 2009, Seidel et al. first reported the observation of enhanced conductivity at 109° and 180° domain walls in insulating multiferroic BFO epitaxial

thin films.[14] The authors ascribed this phenomenon to the intrinsic structural change at the walls, which would give rise to an increased carrier density and/or a decrease in the bandgap within the walls. In 2011, conduction through naturally formed 71° domain walls in BFO thin films was experimentally demonstrated by Noheda et al.[203] The authors found that conduction was provided by n-type carriers and the mechanism for conduction was the same both in domains and at domain walls. This work further suggested that oxygen vacancies would accumulate at the walls and lower the Schottky barrier more in the walls than in the domains, resulting in larger current at the walls. Recently, based on atomic-scale chemical and structural analysis (electron energy loss spectroscopy (EELS) and high-angle annular dark-field (HAADF) imaging), Tadej et al. provided direct evidence of an accumulation of charged defects, i.e., Fe^{4+} cations and bismuth vacancies, at 109° domain walls in BFO.[198] The authors pointed out that the presence of positively charged Fe^{4+} point defects within domain walls is mainly responsible for the conductivity, and the main transport mechanism is p-type hopping involving Fe^{4+} and Fe^{3+}.[198] Further studies are required to settle the debate about the nature of domain-wall conductivity in ferroelectric/multiferroic materials.

Generally, conduction at FEDWs should be avoided as far as possible in order to prevent device failure caused by the enhanced leakage current.[204] Nevertheless, FEDW density or geometry can be electrically controlled and thus opens a new pathway for high-density nonvolatile memory and logic devices.[75,205] The first prototype memory device based on reconfigurable ferroelectric domain walls has been demonstrated by Sharma et al. in 2017 (Figure 5b).[206] The binary ON–OFF states of the device are defined by the existence or absence of conductive walls. As is shown, by bridging two coplanar Pt electrodes on the BFO films as the conductivity pathway under switching bias, the formation of FEDWs (the ON state) can result in a uniform electrical current, as compared to a quite small current in the FEDW-free state (the OFF state). Therefore, memory function can be achieved by utilizing the domain walls conductivity,[207] and demonstrate that FEDWs play an important role in future memory and logic devices.

FEDWs also play a significant role in the anomalous photovoltaic (APV) effect.[18,208–211] The entire field of photoferroelectrics has been revitalized by the reported APV effect in BFO epitaxial thin films in 2009,[18] which corresponds to a very large open-circuit photovoltage (considerably larger than the bandgap of the material). The seminal work from Yang et al. demonstrated that above bandgap photovoltage varies linearly with the total number of domain walls and is obtained only when in-plane electrodes for electric transport measurements run parallel to the stripe domain walls in BFO thin films, while no photovoltage existed when electrodes run perpendicular to the 71° walls.[18] Therefore, the bulk photovoltaic (BPV) effect, which exists in noncentrosymmetric materials, had been ruled out, and the authors attributed the observed APV effect to electrostatic potential steps at FEDWs leading to efficient separation of electrons and holes.[208] However, subsequent experiments by Alexe et al. have shown no enhanced PV effect at FEDWs by using customized PV measurement method and suggested that the BPV effect is solely responsible for the APV effect in BFO.[210] Additionally, the enhanced photoconductivity at DW has been proved due to its intrinsic conductivity.[209] Very recent work from Lindenberg et al. disentangles the contributions of different photovoltaic mechanisms in BFO films.[212] By detecting terahertz radiation emanated by light-induced currents, the authors found that domain-wall driven charge separation is the dominant mechanism in BFO films with periodic stripe domains, whereas the BPV effect dominates in the monodomain BFO films. They further revealed that FEDW-mediated peak photocurrent is two orders of magnitude higher than the BPV-driven bulk shift current.[212] We can see the importance of FEDW plays in the photovoltaic effect, but their exact mechanism is still under debate.

Another significant field of FEDW related research is negative capacitance.[213] Negative capacitance is thermodynamically unstable and thus rare in nature.[214] In 2016, Zubko et al. demonstrated stable negative capacitance over a wide range of temperature in artificial $PbTiO_3/SrTiO_3$ superlattices (Figure 5c).[91] The depolarization field produced by the separation of ferroelectric bound charge from screening charge promotes the formation of 180° domains. Using a combination of phenomenological modeling and second-principles atomistic simulations, the authors suggest that 180° domain walls dominate the dielectric response, their motion not only gives rise to negative permittivity, but also enhance its temperature range. The observed negative capacitance not only provides significant insights into fundamental physics but can also potentially overcome the "Boltzmann tyranny" for energy-efficient transistors.[213]

Besides quasi-static electronic properties, recent work shows that FEDWs can be engineered to achieve tailored dynamic responses in the GHz frequency range (Figure 5d).[215] The FEDWs were considered to be detrimental to the performance of tunable dielectric microwave devices because of high dielectric loss and hysteretic device response under an applied AC electric field.[216] To avoid these effects, ferroelectric materials are often operated above their Curie temperature, where tunability is compromised. Recently, Gu et al., found that strained $Ba_{0.8}Sr_{0.2}TiO_3$ thin films with a high density of domain walls exhibited wide microwave tunability (1–10 GHz) and ultralow loss. The device performance is better than that of state-of-art film devices by a few orders of magnitude and comparable to that of bulk single crystals. Resonant domain wall movement, i.e., oscillations in a sample with rich FEDWs were considered to be the main factors behind the observation of ultralow loss and the exceptionally high-quality factor.

Domain wall density and geometry can be manipulated by external factors, such as electric field,[217] mechanical force,[218] surface chemistry,[219] film thickness,[220] temperature,[221] polarized light,[222] etc., opening the door to novel reconfigurable nanoelectronic devices. For instance, low thermal conductance at domain walls, which inhibiting the transmission of phonons, can act as a dynamic heat modulators by changing the density of domain walls by varying epitaxial strain and film thickness.[17] Moreover, FEDWs in multiferroic thin films were found to exhibit intriguing magnetic properties. For instance, Farokhipoor et al. described a route to synthesize novel 2D ferromagnetic phases induced by the large local stress at the domain walls of hexagonal manganite $TbMnO_3$ epitaxial thin films.[223] This property can be further tuned by changing the fraction of domain walls in epitaxial thin films and providing a potential for spintronic and electronic devices. In ferroelectric

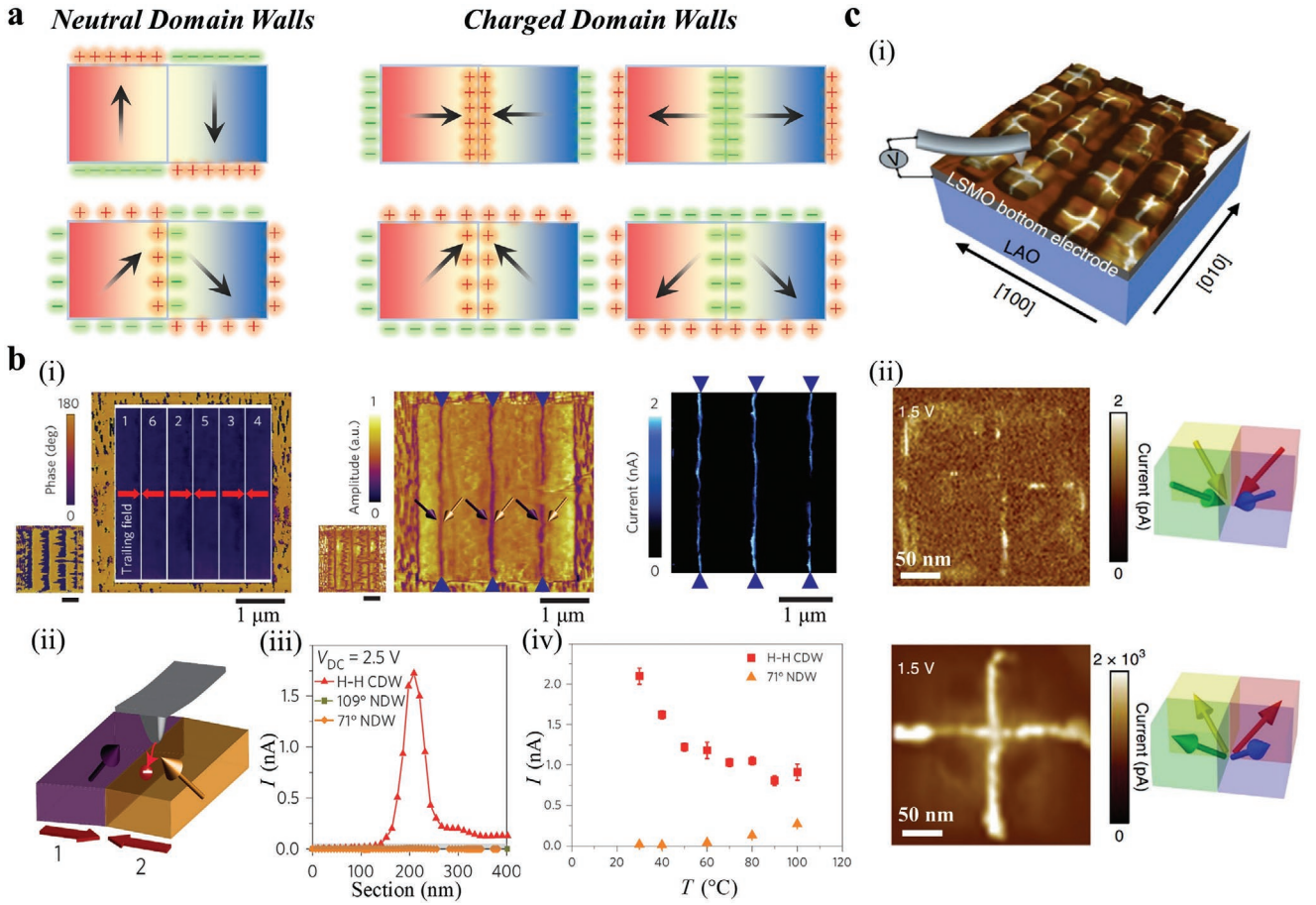

Figure 6. Conduction at charged domain walls in ferroelectric thin films. a) Schematic of neutral domain walls (NDWs) and charged domain walls (CDWs). b) Reliable and repeatable patterning of CDWs with metallic-like conductivity in $(Bi_{0.9}La_{0.1})FeO_3$ epitaxial thin films: i) left, vertical (large image) and lateral (small image) PFM phase micrographs of six regions successively poled up with opposite trailing field directions as indicated by the red arrows. Middle, the corresponding PFM amplitude images. The violet and yellow arrows denote the direction of the polarization in the six regions. The blue arrows point at the position of the head-to-head CDWs. Right, the current map collected at a tip-bottom electrode bias of 2.5 V on the CDWs array shows giant conduction at the head-to-head CDWs; ii) schematic of creating a head-to-head CDW with its corresponding polarization orientations; iii) cross-sectional profile of current maps at the 71°, 109° NDWs and head-to-head CDWs; ii) schematic versus temperature at V_{DC} = 3 V on a head-to-head CDW and a 71° NDW. b) Reproduced with permission.[234] Copyright 2015, Springer Nature. c) Topologically confined CDWs of the self-assembled $BiFeO_3$ nanoislands: i) schematic of the experimental geometry for investigating conduction at the domain walls of BFO nanoislands on $La_{0.7}Sr_{0.3}MnO_3$ on $LaAlO_3$; ii) on the left, the current maps at the domain walls under 1.5 V bias at the initial state and after polarization switching of the islands; on the right, schematic of polarization configuration of center-convergent and center-divergent domain structures in the BFO nanoislands, respectively. c) Reproduced with permission.[75] Copyright 2018, Springer Nature.

antiferromagnet BFO thin films, the FEDWs exhibit enhanced magnetic moment and magnetoresistance.[15,224] Moreover, it is found that the domain walls of BFO play a critical role in exchange coupling between BFO and ferromagnetic metals, wherein pinned uncompensated spins at domain walls give rise to exchange bias in BFO/ferromagnetic metal heterostructures.[225–227] The magnetic/electric coupling property at domain walls open an intriguing territory for electric field control of magnetism and vice versa. Recently, by combining spin dynamic simulations with several characterization techniques, including soft resonant elastic X-ray scattering (REXS), neutron scattering, piezoresponse force microscopy and scanning nitrogen-vacancy magnetometry, Chauleau et al. revealed the presence of both chiral electrical winding and periodic chiral antiferromagnetic texture along the domain walls of BFO epitaxial thin films.[228] The high-density ferroelectric stripe domain network is imprinted onto the antiferromagnetic order, forcing spin cycloids with different propagation vectors to stitch in a chiral knot. The peculiar multiferroic chiral texture tangled at domain walls will open an opportunity for realizing "antiferromagnetic skyrmions," which is tremendously appealing for spintronics.

3.1.2. Charged Domain Walls in Ferroelectric Thin Films

Most observed FEDWs mentioned above meet the condition of electrostatic compatibility and are hence called neutral domain walls (NDWs). NDWs carry no net bound charge and only slightly enhanced conductivity (currents of a few pA) at such uncharged domain walls has been shown.[202,203,229] Besides NDWs, there are walls with nonzero bound charge due to head-to-head convergence or tail-to-tail divergence of spontaneous polarization called as charged domain walls (CDWs) (**Figure 6**a).[230] Bound charges at CDWs generate large electric

fields, making the domain structure energetically costly and unstable. Therefore, CDWs rarely appear naturally in the ferroelectric insulators. However, recently, several research groups have shown the existence of CDWs in various ferroelectrics, such as, $BiFeO_3$,[67] $BaTiO_3$,[200] $Pb(Zr_xTi_{1-x})O_3$,[231] improper ferroelectric $ErMnO_3$,[201] and hybrid improper ferroelectric $(Ca,Sr)_3Ti_2O_7$.[232–237] Their existence is due to a strong screening of the bound charge by enough mobile charged defects and/or free carriers.[233,236] Owning to such screening, the conductivity at CDWs could be several orders of magnitude higher than that of the bulk (up to 13 orders of magnitude enhancement).[200,234,237,238] One prominent example is the reliable and repeatable patterning of CDWs with metallic-like conductivity (i.e., conductivity decreases with increasing temperature) in $(Bi_{0.9}La_{0.1})FeO_3$ epitaxial thin films by Crassous et al. (Figure 6b).[234] The CDWs are created by the "trailing field" present in the triaxial control of a biased AFM tip. The head-to-head CDWs display very high conductivity (current up to ≈1.7 nA at a bias voltage of 2.5 V), more than three orders of magnitude higher than that of NDWs. The authors suggest that the CDWs were compensated by electrons injected from the AFM tip while the walls are being created. Another notable example is the creation and reversible electric-field control of self-assembled, charged domain walls in BFO nanoislands grown on $LaAlO_3$ substrates (Figure 6c).[75] It is found that the tail-to-tail CDWs in the center-divergent states have conductivity three orders of magnitudes higher than those in the head-to-head CDWs in the center-convergent states. More interestingly, unlike most previous studies, the cross-shaped CDWs are topologically confined through careful control of electrostatic and geometric boundary conditions. The stable, highly conductive, electric-field-controllable, 2D CDWs hold great promise for the future development of high dense, low power, high-speed domain wall-based devices.

3.1.3. Domain Walls and Other Topological Defects in Ferroelastics

Twin/domain walls in nonpolar ferroelastics have received considerable attention in the past few years, as they exhibit emergent functionalities, such as ferrielectricity,[239] ferroelectricity,[240] ferromagnetism,[241] large piezoelectric response,[242] electronic conductivity,[243] and even superconductivity.[244] Typical examples are superconductivity in twin walls of insulating WO_3,[244] and spontaneous polarization in twins walls in nonpolar ferroelastics, such as $CaTiO_3$,[239] $SrTiO_3$,[245] and $LaAlO_3$.[246] Besides the 2D topological defects, Salje and Scott have further predicted the existence of 1D topological defects named Bloch lines composed of ordered vortex arrays at chiral Bloch-type polar walls in $SrTiO_3$.[247] Similar topological defects named Ising lines have been predicted to exist within ferroelectric Bloch walls in $BaTiO_3$ by the group of Hlinka.[248] The first experimental observation of Bloch lines in ferroelectric systems was obtained by means of 3D-SHG measurements in periodically poled $LiTaO_3$ in 2017.[73] These low-dimensional topological defects could exhibit exotic functionalities that do not exist in the bulk, which opens the door for using such functional interfaces as active elements in nanoelectronic applications, such as high-density memory devices.[247]

3.2. Flux-Closure/Vortex Domains in Ferroelectric Epitaxial Thin Films and Heterostructures

3.2.1. Flux-Closure Domains in Ferroelectric Thin Films and Heterostructures

Inspired by the topological spin textures in magnets, the search for topological polar structures in ferroelectrics is under intense investigation. One of the main differences between ferroelectrics and ferromagnets is the much larger spontaneous strains accompanied by the ferroic-phase transition for ferroelectrics, which are of the order of $\approx 10^{-2}$ (≈6.5% for $PbTiO_3$, ≈1% for $BaTiO_3$) and $\approx 10^{-5}$ for ferroelectrics and ferromagnets, respectively. The precondition for topological polar structures in ferroelectrics requires continuous rotations of dipoles in each unit cell, which is generally not allowed by crystal symmetry and, thus importantly, will cause larger strains and higher energy cost than the forming of spin textures in ferromagnetics. For this reason, the ferroelectric community started searching the flux-closure/vortex domains in ferroelectrics with smaller spontaneous strains, such as $BaTiO_3$, since the theoretical finding of polar vortices.[64] However, somewhat unexpectedly, the ferroelectric flux-closure domains were experimentally found in $PbZr_{0.2}Ti_{0.8}O_3$, $BiFeO_3$, and $PbTiO_3$ related films/multilayers with large spontaneous strains, where external epitaxial strains and interface compensations contribute to breaking the local ferroelectric symmetries and forming dipole rotations.[59,60,63] It should be emphasized that advanced TEM techniques and related analysis methods are indispensable here for revealing these polar topologies.[193,249,250]

Specifically, in 2011, a single flux-closure structure, with real continuous polarization rotation, at a 180° domain wall/interface triple point was first observed in epitaxial $PbZr_{0.2}Ti_{0.8}O_3$ thin-film grown on a $SrRuO_3$ buffered $SrTiO_3(001)$ substrate using atomic-resolution aberration-corrected TEM.[59,251] On the basis of this technique, researchers were able to produce a vector map of the atomic-polar displacements ($\boldsymbol{P}_{PD}$) from a cross-sectional high-resolution transmission electron microscopy (HR-TEM) image which gives the electric dipole moment for each individual unit cell.[60,69] The Zr/Ti-ion displacement with respect to the adjacent O ion gives the polarization state of $PbZr_{0.2}Ti_{0.8}O_3$. The resulting vector map of dipole moments on the $PbZr_{0.2}Ti_{0.8}O_3$ film showed the flux-closure structure near the 180° domain wall/interface area (**Figure 7**a,b). As is shown, the Zr/Ti shift vector maps directly revealed evidence of continuous dipole rotations which form a flux-closure structure. At almost the same time, using aberration-corrected HAADF-STEM (which can image crystal materials with sub-Angström resolution), vortex nanodomains were observed in the $BiFeO_3/TbScO_3$ heterostructures, where in each vortex, four domains which are allowed by the rhombohedral symmetry of $BiFeO_3$ crystal were identified.[60] The HAADF-STEM imaging could directly record the polar structure of ferroelectrics, via imaging the positive-negative charge separation induced by ion displacement. In the above two cases, the importance of advanced TEM method for directly studying polar topologies have been witnessed.

Later in 2015, strain engineering was further introduced to manipulate possible dipole topologies in ferroelectric

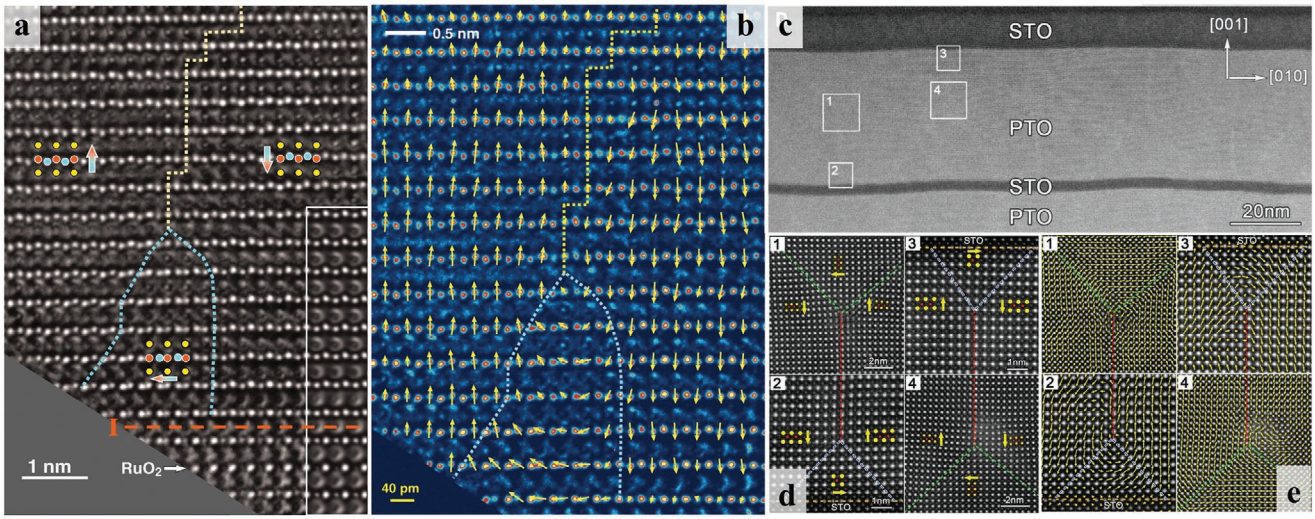

Figure 7. Flux-closure domain in $PbZr_{0.2}Ti_{0.8}O_3$ and flux-closure arrays in $PbTiO_3/SrTiO_3$ multilayer. a) Atomic resolution of cross-sectional image of $PbZr_{0.2}Ti_{0.8}O_3$ layer on $SrRuO_3$ buffered $SrTiO_3$(001) substrate. b) Ti/Zr ion displacement vector mapping (yellow arrows) of the atomic image of (a). a,b) Reproduced with permission.[59] Copyright 2011, American Association for the Advancement of Science. c) A cross-sectional low-magnification STEM image of the $PbTiO_3/SrTiO_3$ multilayer. d) A cross-sectional HAADF-STEM image for four typical areas indicated in upper $PbTiO_3$ layer in (c); e) the superposition of Ti displacement vector mapping with the corresponding atomic images in (d). c–e) Reproduced with permission.[63] Copyright 2015, American Association for the Advancement of Science.

film/multilayer structures. Arrays of regular flux-closure domain within $SrTiO_3$ confined $PbTiO_3$ layers in $SrTiO_3/PbTiO_3$ multilayers grown on $GdScO_3$(110) substrates were directly imaged by advanced HAADF-STEM (Figure 7c–e).[63] In this case, the $GdScO_3$ substrate exerts a tensile strain of ≈1.7% on the $SrTiO_3/PbTiO_3$ multilayers, which is important for rotating dipoles near the $SrTiO_3/PbTiO_3$ interface toward the in-plane direction and thus facilitates the forming of flux-closure arrays. In combination with the $SrTiO_3/PbTiO_3$ interface-driven large depolarization field, arrays of regular flux-closure domains within the $PbTiO_3$ layers formed. The closed dipole structures can be identified by extracting the Ti–Pb ferroelectric displacements. It is seen that the Ti displacement mapping forms a flux-closure quadrant in the area of 1, 2, 3, and 4, which is similar to that of ferromagnetic materials.[25] In addition, large-scale flux-closure arrays were further confirmed.[252] These flux-closure domains in $PbTiO_3$ layers show unique elastic strain behaviors where long range strain gradients up to 10^6 m^{-1} were identified.[63] Moreover, the successful preparation of large scale flux-closure arrays in multilayers will facilitate the preservation of such giant strain gradients, which may trigger novel gradient functional device concepts.[253]

3.2.2. Vortex Domains in Ferrelectric Thin Films and Heterostructures

Motivated by the observation of ferromagnetic vortex structure, the early 2000s saw the emergence of suggestions of similar effects in ferroelectrics.[50–52] Ferroelectric vortex states without an out-of-plane core (Figure 1c) have been theoretically predicted in ferroelectric nanostructures,[51] but long range vortex ordering has not been experimentally observed until very recently.[69] Through the combination of advanced TEM, film deposition and strain engineering techniques, the formation of ordered arrays of vortex pairs in $PbTiO_3$ layers confined by $SrTiO_3$ layers, within $(PbTiO_3)_n/(SrTiO_3)_n$ superlattices grown on $DyScO_3$(110) substrate (**Figure 8**a,b) was identified in 2016.[69] Here the $DyScO_3$ substrate exerts a tensile strain of ≈1.2% on the $SrTiO_3/PbTiO_3$ superlattices, where the thicknesses of each $PbTiO_3$ are about 10 unit cells. Chirality was further confirmed for these vortex pairs by resonant soft X-ray diffraction, where a spiral-like polar structure was revealed with left- and right-handed signatures.[89] As seen in the left of Figure 8a, it shows a vector map of the atomic polar displacement ($\boldsymbol{P}_{PD}$) on the cross-sectional HAADF-STEM image for a $(PbTiO_3)_{10}/(SrTiO_3)_{10}$ superlattice, which could reveal the polarization distributions in each $PbTiO_3$ layer.[60] The vector map of these polar displacements indicates the formation of long-range arrays of clockwise (CW) and counter clockwise (CCW) vortex pairs in each $PbTiO_3$ layer of the superlattice. A single CW–CCW vortex pairs is shown in the magnified image (right of Figure 8a), which shows the continuous rotation of local polarization in each unit cell within the CW–CCW vortex pairs. The lateral periodicity of this pair is approximately ≈ 10 nm (from CW to the next CW or vice-versa). Figure 8b shows the 3D structure of CW–CCW array of vortex in $(PbTiO_3)_{10}/(SrTiO_3)_{10}$ superlattice from phase-field simulations (on the right),[69] with experimental HAADF-STEM results where cross-sectional and planar-view DF-TEM images are projected on the same 3D axes (on the left). Red/blue color scales correspond to the curl of the polarization extracted from the phase-field model and the HAADF-STEM polar displacement map ($\mathbf{P}_{PD}$).

The phenomenon of negative capacitance is very rare in nature. Emergent negative capacitance has been directly observed by Salahuddin et al. in $(PbTiO_3)_n/(SrTiO_3)_n$ superlattices with polar-vortex structures.[92] The authors successfully mapped the distribution of electric field and polarization

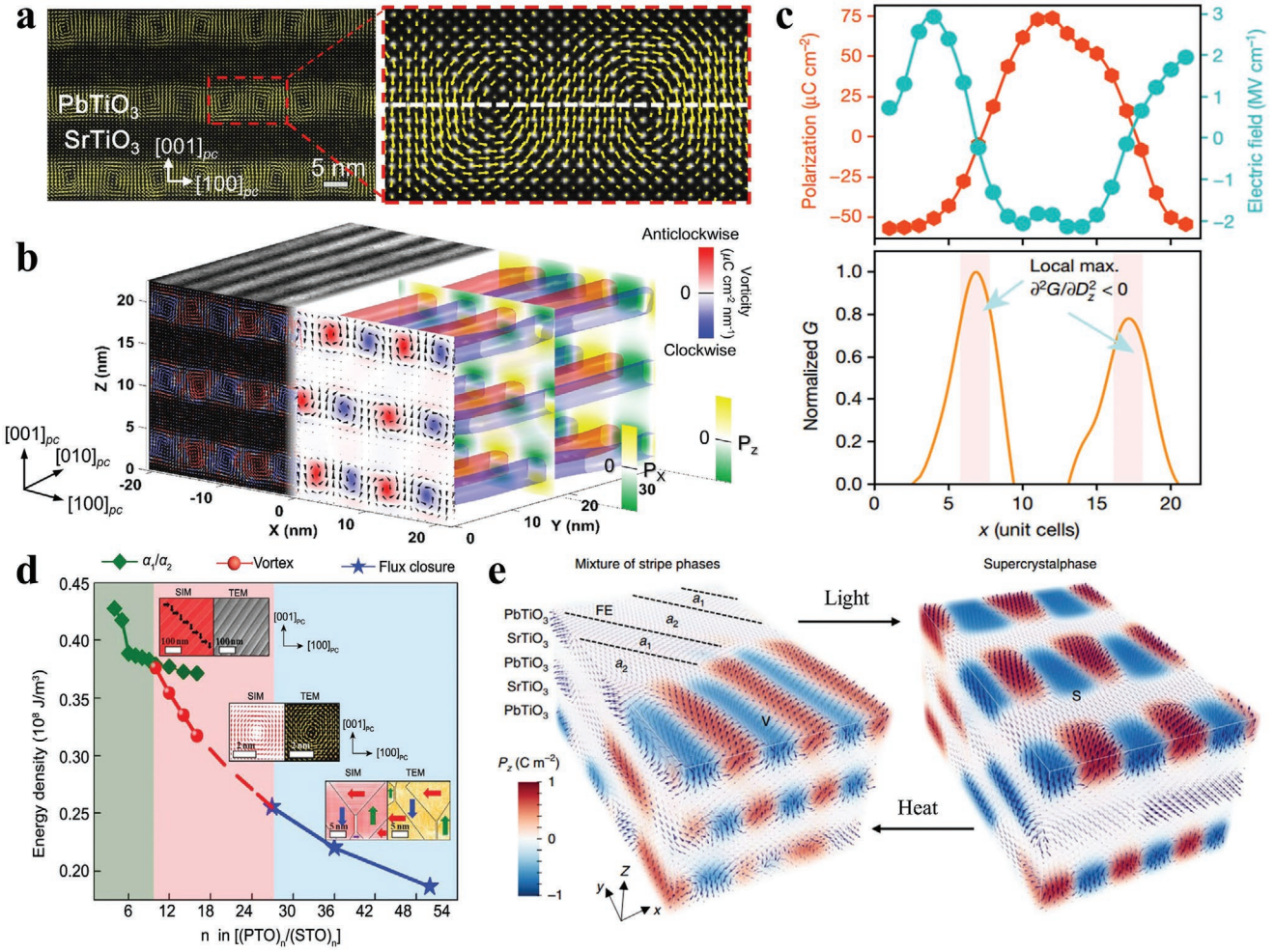

Figure 8. Vortex pairs arrays in $(PbTiO_3)_n/(SrTiO_3)_n$ superlattices. a) (left) A vector map of the atomic polar displacement on the cross-sectional HAADF-STEM image for a $(PbTiO_3)_{10}/(SrTiO_3)_{10}$ superlattices. (Right) A single magnified CW–CCW vortex pair. b) 3D structure of CW–CCW array of vortex in $(PbTiO_3)_{10}/(SrTiO_3)_{10}$ superlattice from phase field simulation (on the right), with experimental HR-STEM studies (on the left). a,b) Reproduced with permission.[69] Copyright 2016, Springer Nature. c) (Top) Polarization component P_z (red hexagons) and electric field component E_z (blue circles) in a CW–CCW vortex pair along the direction of a transverse line across their cores. (Bottom) Energy density obtained from P_z and E_z along this transverse line. Reproduced with permission.[92] Copyright 2019, Springer Nature. d) Phase diagram and total energy density for the $(PbTiO_3)_n/(SrTiO_3)_n$ superlattices grown on $DyScO_3$ substrate. Reproduced with permission.[254] Copyright 2017, American Chemical Society. e) Optical and thermal field manipulation between coexistence phase and superlattice phase. Reproduced with permission.[255] Copyright 2019, Springer Nature.

simultaneously using advanced TEM complemented by phase-field and first-principles-based (second-principles) simulations. According to Landau–Devonshire–Ginzburg theory, stable states in a ferroelectric phase correspond to a double-degenerate free-energy landscape between total free energy G and electric displacement D. Only if the permittivity $\varepsilon \propto \frac{\partial^2 G}{\partial^2 D} < 0$, does negative capacitance appear. In Figure 8c, the polarization component P_z (red hexagons) and electric field component E_z (blue circles) in a CW–CCW vortex pair similar to that in Figure 8a along the direction of a transverse line across their cores have been exhibited on the top. Furthermore, the corresponding energy density obtained from P_z and E_z along this transverse line is shown in the bottom. The area indicated by the arrows has negative curvature, which means the negative capacitance exists in CW–CCW vortex pair arrays in ferroelectric superlattice.

In addition, phase field simulations elucidated that the size confinement is one of the key parameters for stabilizing such topological structures. Phase-field simulations on $(PbTiO_3)_n/(SrTiO_3)_n$ superlattices (n is number of monolayers) on $DyScO_3(110)$ substrates (Figure 8d) indicate that,[254] in short period ($n < 10$) superlattices, the ferroelectric phase is stable, where the emergence of common a_1/a_2 domain structures could be identified.[84] Relatively large period ($n > 25$) superlattices will form a flux-closure pattern.[63,254] In intermediate period ($10 \leq n \leq 25$) superlattices, the model suggested that the formation of exotic topological structures like vortex pairs, by interplay of the elastic, electrostatic, and gradient energies.[69] On the basis of both the experimental results and the phase-field simulations, the vortex structure results (primarily) from competition between three energies—elastic energy ($PbTiO_3$ layers in tensile strain on $DyScO_3$ substrate), electrostatic

energy from built-in field (large polar discontinuity at the interfaces from $PbTiO_3$ to $SrTiO_3$ layers), and gradient energy (the energy required to rotate or change the direction or magnitude of the polarization). The emergent chirality identified in these ordered arrays of polar vortex phase indicates that complex polar topologies similar to those of ferromagnetic materials can also be achieved,[89,90] which encourages further exploring of other types of polar topologies in ferroelectrics, such as polar bubbles and skyrmions.

In particular, new phase transitions related to this polar-vortex phase, stimulated by electric field or laser,[255,256] were identified experimentally recently. In 2017, the experimental observation of emergent coexistence phase of vortex array and in-plane a_1/a_2 domain has been reported in PTO/STO superlattices.[256] After the application of electric field to this coexistence phase system, the interconversion between high-temperature vortex phase and low-temperature stripe phase (a_1/a_2 domain) can be realized, meanwhile the corresponding piezoelectric and nonlinear optical responses changed dramatically.[256] In 2019, it is found that the phase transitions between the coexistence phase and a new so-called 3D superlattice phase in PTO/STO superlattice can occur reversibly by optical and thermal manipulation (Figure 8e). The coexistence phase including in-plane a_1/a_2 domain and vortex pair arrays would be converted to a single 3D superlattice phase by optical pulses, while thermal annealing can reverse this process entirely.[255] These findings indicate abundant multifield coupling controllability and novel physical properties to be explored in ferroelectric polar vortex states. The glassy behavior and extremely "soft" nature of the polarization in the vortices could enable large field-tunable and collective response in $PbTiO_3/SrTiO_3$ heterostructures.

3.3. Nanobubble Domains in Ferroelectric Heterostructures

Topological defects like bubble domains are widely studied in magnetic systems.[257] Ferroelectric bubble domains (i.e., laterally confined spheroids of sub-10 nm size with local dipoles self-aligned in a direction opposite to the macroscopic polarization of a surrounding ferroelectric matrix) can be considered a precursor to polar skyrmions, and thus are both fundamentally and technologically exciting in condensed matter physics. In 2004, using first-principles calculations, Bellaiche et al. first predicted the existence of nanobubble domains in epitaxial $Pb(Zr_{0.5}Ti_{0.5})O_3$ ultrathin films.[51,258] Until 2017, Zhang et al. first experimentally demonstrated the nanoscale bubble domains in an ultrathin structured ferroelectric film [7 unit cell $PbZr_{0.2}Ti_{0.8}O_3$/2 unit cell $SrTiO_3$/7 unit cell $PbZr_{0.2}Ti_{0.8}O_3$ (PZT/STO/PZT)] by tuning its depolarization field via an STO spacer layer (**Figure 9**a).[78] The existence of the bubble domains is revealed by high-resolution piezoresponse force microscopy (PFM) (Figure 9b), and is corroborated by aberration-corrected atomic-resolution scanning transmission electron microscopy mapping of the polarization displacements (Figure 9c). The vertical PFM amplitude image shows the two different size domain topologies. One type of domains is larger than ≈10 nm (marked by white dashed arrows) with distinct domain wall separated by up and down domain states, distinguished as cylindrical bubble

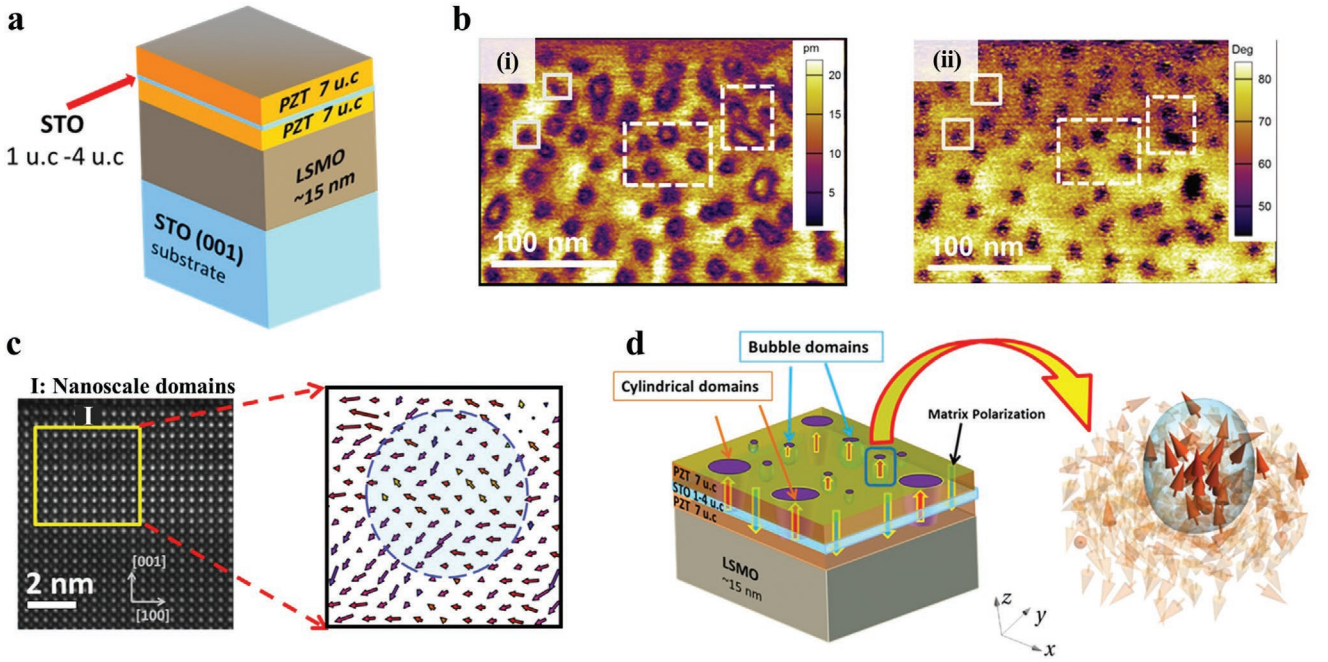

Figure 9. Nanobubble domain structures in $PbZr_{0.2}Ti_{0.8}O_3/SrTiO_3/PbZr_{0.2}Ti_{0.8}O_3$ (PZT/STO/PZT) heterostructure. a) Schematic description of the PZT/STO/PZT heterostructure. b) Piezoelectric force microscopy: i) amplitude and ii) phase images of PZT/STO/PZT heterostructure with 2 u.c. STO spacer showing existence of bubble domains with fussy domain walls (white boxes) and cylindrical domains with clear domain walls (white dashed boxes). c) Cross-sectional STEM high angle annular dark-field (HAADF) images of the heterostructure (left) and corresponding polarization displacement mapping of yellow region (right) shows a distinct topologies of bubble domain. d) Monte Carlo simulations of nanoscale domains inside the films. The blue box indicates the bubble domains and the calculated dipolar structure of this bubble domain (right). a–d) Reproduced with permission.[78] Copyright 2017, Wiley-VCH.

domains. Another type of domains is ultrasmall (<10 nm) appears as a dark spot due to the PFM resolution limit, which distinguished as spheroid bubble domains. The corresponding PFM phase images clearly reveals that this nanobubble domain has different phase contrast than the surrounding regions and has phase contrast less than 180°. The cross-sectional atomic-scale high-resolution scanning transmission electron microscopy (HR-STEM) image confirms sharp and coherent interfaces of the heterostructure and identified the distinct bubble topology region. The polarization structure of ultrathin films was further confirmed by Monte-Carlo simulations (Figure 9d).[78] Unlike regular cylindrical domains with uniform distribution of polarization, the bubble domains exhibit polarization rotation with mixed Néel–Bloch character. The size of the ferroelectric bubble domains (<10 nm) is much smaller than their ferromagnet counterparts, makes them exciting for applications in nanoelectronics and logic devices.[257] In addition, an enhancement of piezoelectricity during the irreversible phase transition from labyrinthic domains to nanobubble domains was also demonstrated. Recently, the deterministic and reversible transformation of bubble domains into cylindrical domains using a scanning probe microscopy (SPM) approach was demonstrated by the same group.[259] The bubble domain state can be created by an electrical pulse with a specific combination of amplitude and duration, meanwhile it can be erased by a mechanical force via the AFM tip. This pathway for switching between various topological defects holds promise for emergent devices. Altogether, the observed nanobubbles highlight the richness of polar topologies possible in ultrathin ferroelectric heterostructures as a result of interplay between elastic and electrostatic energies.[82]

3.4. Polar Skyrmions in Ferroelectric Superlattices

So far, skyrmion as a critical noncoplanar vortex topological structure has been widely studied in magnetic materials. This topological texture has been found to be essentially stable due to the chiral interactions in ferromagnetic films. On the other hand, the absence of such chiral interactions in ferroelectrics has led to the existence of polar skyrmions being questioned and rarely studied. Until very recently, progress has been made in the discovery of stable polar skyrmion structure in ferroelectric material both in theory and experiment. In 2015, using a first-principles-derived effective-Hamiltonian approach, Bellaiche et al. first predicted the existence of skyrmionic state in $BaTiO_3/SrTiO_3$ nanocomposites with a cylindrical $BaTiO_3$ (BTO) nanowire embedded in a $SrTiO_3$ (STO) square matrix (**Figure 10**a–d).[82] Due to the distinct difference in magnitude of polarization in BTO and STO, under a certain critical electric field, the polarization P_z in BTO would be earlier reversed from upward to downward than that in STO. In Figure 10b, the skyrmion charge ($Q = 1$) as an integral of Pontriagin density (q) is decomposed into fractions (narrow peaks) with equal contributions at the domain wall junction. The upward (downward) peak represents positive (negative) contribution to the total topological charge. The polarization of stable skyrmion obtained from simulations at 15 K and a line of dipoles along x across the core of skyrmion is shown in Figure 10c. We can see a polar skyrmionic state is stabilized in the BTO/STO composites under a threshold electric field. The temperature dependence of the threshold electric field inducing the system from vortex state to skyrmionic state is depicted in Figure 10d. Therefore, the stable existence of skyrmion can be realized in ferroelectric materials by geometrically induced chiral interaction. In spite of no intrinsic chiral interactions in ferroelectric materials, ferroelectric skyrmions indeed can be constructed and stabilized by extrinsic chiral interactions, which can be induced by means of constrained geometry, dipole interaction with external strain/electric fields, etc. In 2018, Hong et al. predicted the presence of polar skyrmion bubbles in $PbTiO_3/SrTiO_3$ superlattice driven by external electric field using phase-field simulations.[260] In 2019, using second-principles simulations, Gonçalves et al. proposed an original approach to create the polar skyrmions by harnessing the Bloch-type 180°domain walls at low temperature in prototype ferroelectric $PbTiO_3$.[261] The authors further predicted that such polar skyrmions can be controlled by external stimuli, such as temperature, electric field and epitaxial strain. For instance, a topological transition between skyrmionic ($N = 1$) and normal nanodomain ($N = 0$) states occurs at 235 K. These theoretical studies inspired and guided the experimental searching for polar skyrmions in ferroelectrics.

Further interplay of elastic, electrostatic, and gradient energies in similar systems have shown potentials to mediate an even more complex swirling topological feature—polar skyrmions (equivalent of magnetic skyrmions) has been observed in $(PbTiO_3)_n/(SrTiO_3)_n$ heterostructures grown on $SrTiO_3(001)$ substrates with small lattice-mismatch strain.[83] Looking down at the surface of the $(PbTiO_3)_{16}/(SrTiO_3)_{16}$ superlattice structure, plan-view HAADF-STEM images (Figure 10e) revealed long-range ordered arrays of circular features with size of ≈8–9 nm, suggesting that this polar order extend through the film over many tens of nanometers length scale. Low-resolution, cross-sectional DF-TEM imaging (blue shaded $PbTiO_3$ layer in Figure 10e), in turn, revealed a pseudo-long-range periodic array of intensity modulations along both in- and out-of-plane directions of the superlattice, corresponding to a cylindrical domain with antiparallel (up–down) polarization. The reversed titanium displacement is converging from the edge to the center, corresponding to a hedgehog-like (Néel-type) skyrmion structure (Figure 10f). Moreover, 4D STEM (4D-STEM) with an electron microscope pixel array detector (EMPAD) provides the information at the central $PbTiO_3$ layers.[262] In 4D-STEM, the full momentum distribution, that is, the electron diffraction pattern, was collected at every scan position by the EMPAD. From the diffraction patterns collected on the EMPAD, reconstructed the low-angle annular dark-field (ADF) image (Figure 10g) and the probability current flow in x and y giving the vector components of polar order (Figure 10h) of $(PbTiO_3)_{16}/(SrTiO_3)_{16}$ superlattice, which is largely weighted toward the Bloch-like skyrmion in the middle of the $PbTiO_3$ layer. In Figure 10i, the combination of hedgehog and Bloch skyrmion has been further confirmed by second-principles *ab* initio calculations.[263] These calculations showed that the local electric dipoles continuously rotate both in- and out-of-plane at the $PbTiO_3/SrTiO_3$ boundary. Moreover, resonant soft-X-ray diffraction experiments show strong circular dichroism at the Ti-L_3 edge, confirming emergent chiral nature of the structure, consistent with the presence of Bloch domain walls.[83] In summary, the observations of polar skyrmions, and

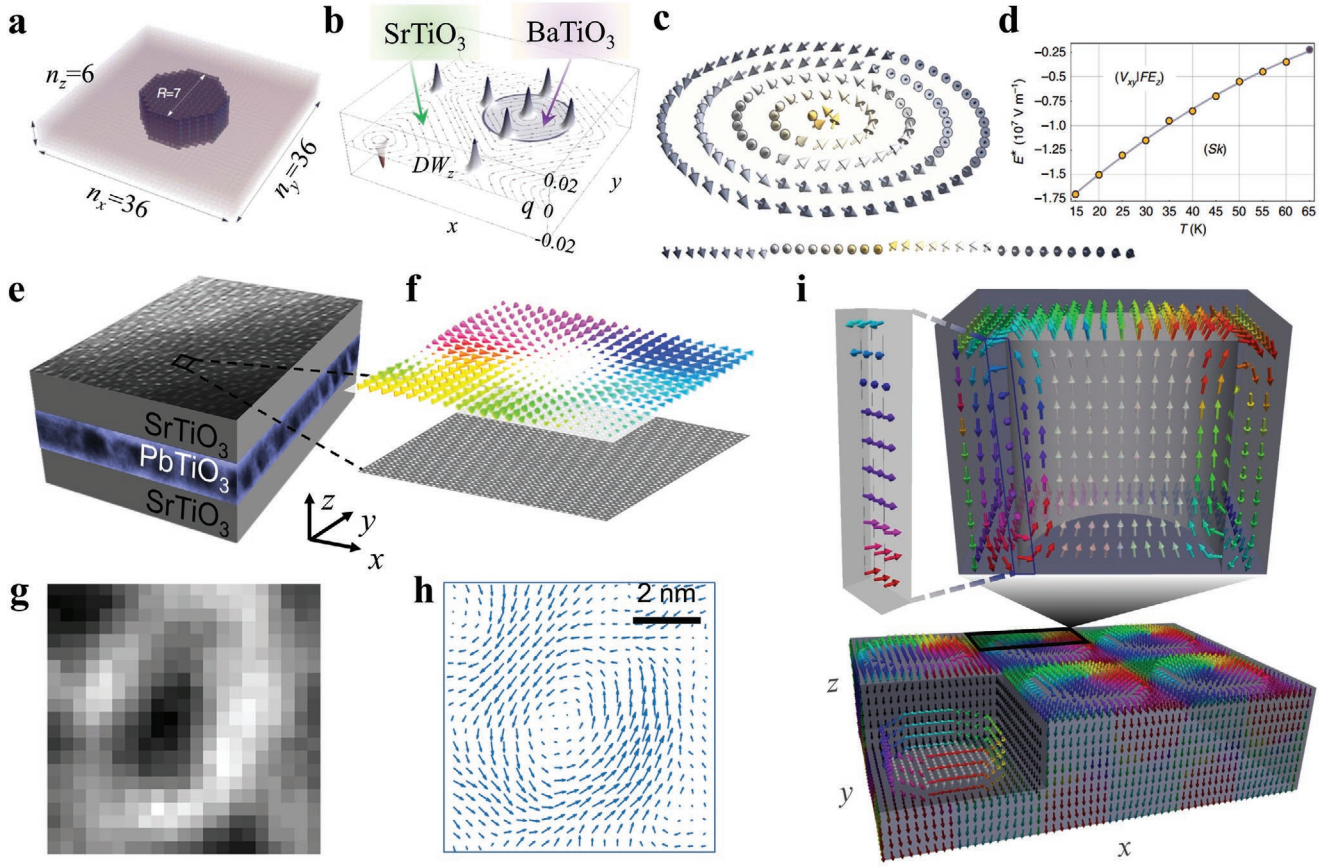

Figure 10. Theoretical prediction and experimental observation of polar skyrmions in ferroelectric materials. a–d) Stable skyrmionic state in $BaTiO_3$/$SrTiO_3$ nanocomposites. a) Schematics of nanocomposites with a cylindrical $BaTiO_3$ (BTO) nanowire embedded in a $SrTiO_3$ (STO) square matrix. b) Topological charge density of the polar skyrmion. c) (Top) Polarization of stable skyrmion obtained from simulations at 15 K. (Bottom) A line of local dipoles along *x* across the core of skyrmion. d) Temperature dependence of the threshold electric field leading to skyrmionic state. a–d) Reproduced under the terms of the CC-BY Creative Commons Attribution 4.0 International License (https://creativecommons.org/licenses/by/4.0).[82] Copyright 2015, Springer Nature. e–i) Experimental observation of polar skyrmions in $PbTiO_3$/$SrTiO_3$ superlattice. e) A sketch covered with a planar-view dark-field TEM image in the top and two cross-sectional-view dark-field TEM images in the lateral of the superlattice. f) Hedgehog-like polarization distribution implies the presence of an Néel-type skyrmion. The top is a reversed Ti-displacement vector map, corresponding to the bottom with an atomically resolved planar-view HAADF-STEM image of an individual skyrmion bubble. g) The low-angle annular dark-field (ADF) image from the 4D-STEM image of a $[(PbTiO_3)_{16}/(SrTiO_3)_{16}]_8$ superlattice. h) Possible current flow of polarization map from the 4D-STEM above. i) Global (bottom) and local (top) distribution of polar skyrmion lattice in $PbTiO_3$/$SrTiO_3$ superlattice from second-principles simulations. e–i) Reproduced with permission.[83] Copyright 2019, Springer Nature.

all above mentioned polar topologies indicate that complex polar structures resembling those of magnets could be achieved by fine adjusting of elastic, electrostatic and gradient energies.

4. Summary and Outlook

The last decade has witnessed significant developments in the study and understanding of topological structures in ferroic thin films and heterostructures. The topological spin/polar textures are stable at the nanoscale and have exotic properties different from the bulk. Along with gaining fundamental knowledge about the new topologies, understanding, and controlling these new structures can lead to new technological applications, such as high-density, low-power, fast-speed memory, and logic devices. The research on topological structures in ferroic thin films and heterostructures, however, is still in its infancy and thus there remain many open questions, such as

1) Topological patterns like magnetic skyrmions have garnered enormous potential applications in the design of magnetic racetrack memories.[141,264,265] On the other hand, the recent discovery of polar vortices and bubbles/skyrmions in ferroelectric is of profound fundamental importance and poses new lines of research. In future works, we should study the dynamic evolution of the polar topologies under external stimuli, such as electric field, mechanical force, optical light, etc. If the polar topologies can move with electric field, one can use to create novel nonvolatile electric "racetrack memory" devices. Moreover, the stabilization of such nonuniform polar textures could provide highly enhanced and tunable susceptibilities, steady state negative capacitance, and other unexpected properties, such as conductivity or magnetism, which will be a pathway for engineering novel functionalities previously inaccessible in these materials.
2) The nature and mechanisms of the possible magnetic skyrmions and THE in magnetic oxide thin films and

heterostructures needs to be determined by more reliable characterization tools with adequate resolution, such as LTEM, and requires more input from theoretical studies on the electronic structure of the oxide system.

3) Are there other polar topologies, such as merons, hopfions,[266] etc., as well as the topological phase transition possible in ferroelectric thin films and heterostructures? The realization of such questions will require considerable advanced synthesis, characterization, and computational approaches to explore this complex, diverse landscape.
4) Another important area is the investigations on the controlled chirality of polar skyrmions/vortices in ferroelectric thin films and heterostructures.[267] A significant challenge in the coming years will be how to write and read the chirality of the spin/polarization topologies on the nanoscale by using an electric-field manner that can be easily integrated into the modern devices.
5) The generation of topological textures could be extended to other material systems and symmetries (such as asymmetric or tricolor superlattices).[268] For example, there has been very limited work on the coexistence of polar and spin topologies and their coupling effects in multiferroic thin films and heterostructures, such as multiferroic Cu_2OSeO_3[38] thin films and $BiFeO_3$-based superlattices. One can expect that the manipulation of the topological polar textures could greatly influence the magnetic order parameter and vice versa in multiferroics. We believe that this could be an area of strong focus in the future.

Acknowledgements

S.Q.C., S.Y., and Z.P.H. contributed equally to this work. Z.H.C. thanks Dr. Sujit Das and Dr. Xichao Zhang for useful discussions. Z.H.C. acknowledges the support from the National Natural Science Foundation of China (Grant Nos. 51802057 and U1932116) and Guangdong Basic and Applied Basic Research Foundation (Grant No. 2020B1515020029). Z.P.H. acknowledges the support from the National Natural Science Foundation of China (Grant Nos. 51901081, 11574091), Science and Technology Program of Guangzhou (No. 2019050001). Y.L.T. acknowledges the Youth Innovation Promotion Association CAS (Grant No. 2016177). W.Z. acknowledges Shenzhen Science and Technology Program (Grant No. KQTD20170809110344233) and Bureau of Industry and Information Technology of Shenzhen through the Graphene Manufacturing Innovation Center (201901161514). L.C. acknowledges the support from the National Natural Science Foundation of China (Grant No. 51972160), the Science and Technology Research Items of Shenzhen (Grant Nos. JCYJ20170412153325679 and JCYJ20180504165650580), High-Level Special Funding (Nos. G02206303 and G02206403). Work at Berkeley was supported by the U.S. Department of Energy, Office of Science, Office of Basic Energy Sciences, Materials Sciences and Engineering Division under Contract No. DE-AC02-05-CH11231 (Materials Project program KC23MP), the U.S. Department of Energy, Office of Science, Office of Basic Energy Sciences, under Award Number DE-SC-0012375, and the National Science Foundation under Grants OISE-1545907, DMR-1608938, and DMR-1708615.

Note: The acknowledgements section was updated on February 9, 2021, after initial publication online.

Conflict of Interest

The authors declare no conflict of interest.

Keywords

ferroelectrics, heterostructures, magnetic materials, multiferroics, thin films, topological structures

Received: February 6, 2020
Revised: April 17, 2020
Published online: August 19, 2020

[1] N. D. Mermin, *Rev. Mod. Phys.* **1979**, *51*, 591.
[2] F. D. M. Haldane, *Rev. Mod. Phys.* **2017**, *89*, 040502.
[3] J. M. Kosterlitz, *Rev. Mod. Phys.* **2017**, *89*, 040501.
[4] J. Seidel, *Nat. Mater.* **2019**, *18*, 188.
[5] R. Wiesendanger, *Nat. Rev. Mater.* **2016**, *1*, 16044.
[6] A. A. Belavin, A. M. Polyakov, *JETP Lett.* **1975**, *22*, 245.
[7] A. Fert, N. Reyren, V. Cros, *Nat. Rev. Mater.* **2017**, *2*, 17031.
[8] X. Zhang, Y. Zhou, K. Mee Song, T.-E. Park, J. Xia, M. Ezawa, X. Liu, W. Zhao, G. Zhao, S. Woo, *J. Phys.: Condens. Matter* **2020**, *32*, 143001.
[9] J. F. Scott, *Science* **2007**, *315*, 954.
[10] S. S. Parkin, in *Advances in Condensed Matter Science*, Vol. *292* (Ed.: T. S. S. Maekawa), Taylor & Francis, London, UK **2002**.
[11] L. E. C. A. K. Tagantsev, J. Fousek, *Domains in Ferroic Crystals and Thin Films*, Springer, New York **2010**.
[12] M. Dawber, K. M. Rabe, J. F. Scott, *Rev. Mod. Phys.* **2005**, *77*, 1083.
[13] G. Catalan, J. Seidel, R. Ramesh, J. F. Scott, *Rev. Mod. Phys.* **2012**, *84*, 119.
[14] J. Seidel, L. W. Martin, Q. He, Q. Zhan, Y. H. Chu, A. Rother, M. E. Hawkridge, P. Maksymovych, P. Yu, M. Gajek, N. Balke, S. V. Kalinin, S. Gemming, F. Wang, G. Catalan, J. F. Scott, N. A. Spaldin, J. Orenstein, R. Ramesh, *Nat. Mater.* **2009**, *8*, 229.
[15] M. Daraktchiev, G. Catalan, J. F. Scott, *Phys. Rev. B* **2010**, *81*, 224118.
[16] Y. Geng, N. Lee, Y. J. Choi, S. W. Cheong, W. Wu, *Nano Lett.* **2012**, *12*, 6055.
[17] E. Langenberg, D. Saha, M. E. Holtz, J.-J. Wang, D. Bugallo, E. Ferreiro-Vila, H. Paik, I. Hanke, S. Ganschow, D. A. Muller, L.-Q. Chen, G. Catalan, N. Domingo, J. Malen, D. G. Schlom, F. Rivadulla, *Nano Lett.* **2019**, *19*, 7901.
[18] S. Yang, J. Seidel, S. Byrnes, P. Shafer, C.-H. Yang, M. Rossell, P. Yu, Y.-H. Chu, J. Scott, J. Ager III, L. Martin, R. Ramesh, *Nat. Nanotechnol.* **2010**, *5*, 143.
[19] J. M. Gregg, *Ferroelectrics* **2012**, *433*, 74.
[20] J. Seidel, R. K. Vasudevan, N. Valanoor, *Adv. Electron. Mater.* **2016**, *2*, 1500292.
[21] S. Das, A. Ghosh, M. R. McCarter, S.-L. Hsu, Y.-L. Tang, A. R. Damodaran, R. Ramesh, L. W. Martin, *APL Mater.* **2018**, *6*, 100901.
[22] G. Tian, W. Yang, D. Chen, Z. Fan, Z. Hou, M. Alexe, X. Gao, *Natl. Sci. Rev.* **2019**, *6*, 684.
[23] H.-B. Braun, *Adv. Phys.* **2012**, *61*, 1.
[24] N. Nagaosa, Y. Tokura, *Nat. Nanotechnol.* **2013**, *8*, 899.
[25] C. Kittel, *Rev. Mod. Phys.* **1949**, *21*, 541.
[26] R. D. Gomez, T. V. Luu, A. O. Pak, K. J. Kirk, J. N. Chapman, *J. Appl. Phys.* **1999**, *85*, 6163.
[27] T. Shinjo, T. Okuno, R. Hassdorf, K. Shigeto, T. Ono, *Science* **2000**, *289*, 930.
[28] A. Wachowiak, J. Wiebe, M. Bode, O. Pietzsch, M. Morgenstern, R. Wiesendanger, *Science* **2002**, *298*, 577.
[29] A. P. Malozemoff, J. C. Slonczewski, *Magnetic Domain Walls in Bubble Materials*, Academic Press, New York **1979**.
[30] J. Nielsen, *IEEE Trans. Magn.* **1976**, *12*, 327.

[31] C. Moutafis, S. Komineas, J. A. C. Bland, *Phys. Rev. B* **2009**, *79*, 224429.
[32] A. N. Bogdanov, D. A. Yablonskii, *Sov. Phys. JETP* **1989**, *68*, 101.
[33] S. Mühlbauer, B. Binz, F. Jonietz, C. Pfleiderer, A. Rosch, A. Neubauer, R. Georgii, P. Böni, *Science* **2009**, *323*, 915.
[34] J. Matsuno, N. Ogawa, K. Yasuda, F. Kagawa, W. Koshibae, N. Nagaosa, Y. Tokura, M. Kawasaki, *Sci. Adv.* **2016**, *2*, e1600304.
[35] X. Z. Yu, Y. Onose, N. Kanazawa, J. H. Park, J. H. Han, Y. Matsui, N. Nagaosa, Y. Tokura, *Nature* **2010**, *465*, 901.
[36] X. Z. Yu, N. Kanazawa, Y. Onose, K. Kimoto, W. Z. Zhang, S. Ishiwata, Y. Matsui, Y. Tokura, *Nat. Mater.* **2011**, *10*, 106.
[37] S. Heinze, K. von Bergmann, M. Menzel, J. Brede, A. Kubetzka, R. Wiesendanger, G. Bihlmayer, S. Blugel, *Nat. Phys.* **2011**, *7*, 713.
[38] S. Seki, X. Z. Yu, S. Ishiwata, Y. Tokura, *Science* **2012**, *336*, 198.
[39] I. Raičević, D. Popović, C. Panagopoulos, L. Benfatto, M. B. Silva Neto, E. S. Choi, T. Sasagawa, *Phys. Rev. Lett.* **2011**, *106*, 227206.
[40] W. J. Jiang, P. Upadhyaya, W. Zhang, G. Q. Yu, M. B. Jungfleisch, F. Y. Fradin, J. E. Pearson, Y. Tserkovnyak, K. L. Wang, O. Heinonen, S. G. E. te Velthuis, A. Hoffmann, *Science* **2015**, *349*, 283.
[41] K.-Y. Meng, A. S. Ahmed, M. Bacani, A.-O. Mandru, X. Zhao, N. Bagues, B. D. Esser, J. Flores, D. W. McComb, H. J. Hug, F. Yang, *Nano Lett.* **2019**, *19*, 3169.
[42] S. Woo, *Nature* **2018**, *564*, 43.
[43] A. K. Nayak, V. Kumar, T. Ma, P. Werner, E. Pippel, R. Sahoo, F. Damay, U. K. Rößler, C. Felser, S. S. P. Parkin, *Nature* **2017**, *548*, 561.
[44] X. Z. Yu, W. Koshibae, Y. Tokunaga, K. Shibata, Y. Taguchi, N. Nagaosa, Y. Tokura, *Nature* **2018**, *564*, 95.
[45] F. P. Chmiel, N. Waterfield Price, R. D. Johnson, A. D. Lamirand, J. Schad, G. van der Laan, D. T. Harris, J. Irwin, M. S. Rzchowski, C. B. Eom, P. G. Radaelli, *Nat. Mater.* **2018**, *17*, 581.
[46] W. Legrand, D. Maccariello, F. Ajejas, S. Collin, A. Vecchiola, K. Bouzehouane, N. Reyren, V. Cros, A. Fert, *Nat. Mater.* **2020**, *19*, 34.
[47] C. Phatak, A. K. Petford-Long, O. Heinonen, *Phys. Rev. Lett.* **2012**, *108*, 067205.
[48] S. Wintz, C. Bunce, A. Neudert, M. Körner, T. Strache, M. Buhl, A. Erbe, S. Gemming, J. Raabe, C. Quitmann, J. Fassbender, *Phys. Rev. Lett.* **2013**, *110*, 177201.
[49] N. Gao, S. G. Je, M. Y. Im, J. W. Choi, M. Yang, Q. Li, T. Y. Wang, S. Lee, H. S. Han, K. S. Lee, W. Chao, C. Hwang, J. Li, Z. Q. Qiu, *Nat. Commun.* **2019**, *10*, 5603.
[50] H. Fu, L. Bellaiche, *Phys. Rev. Lett.* **2003**, *91*, 257601.
[51] I. Kornev, H. Fu, L. Bellaiche, *Phys. Rev. Lett.* **2004**, *93*, 196104.
[52] I. I. Naumov, L. Bellaiche, H. Fu, *Nature* **2004**, *432*, 737.
[53] S. Prosandeev, L. Bellaiche, *Phys. Rev. B* **2007**, *75*, 094102.
[54] I. Naumov, A. M. Bratkovsky, *Phys. Rev. Lett.* **2008**, *101*, 107601.
[55] M. G. Stachiotti, M. Sepliarsky, *Phys. Rev. Lett.* **2011**, *106*, 137601.
[56] T. Shimada, X. Wang, Y. Kondo, T. Kitamura, *Phys. Rev. Lett.* **2012**, *108*, 067601.
[57] J. Hong, G. Catalan, D. N. Fang, E. Artacho, J. F. Scott, *Phys. Rev. B* **2010**, *81*, 172101.
[58] A. Gruverman, D. Wu, H. J. Fan, I. Vrejoiu, M. Alexe, R. J. Harrison, J. F. Scott, *J. Phys.: Condens. Matter* **2008**, *20*, 342201.
[59] C.-L. Jia, K. W. Urban, M. Alexe, D. Hesse, I. Vrejoiu, *Science.* **2011**, *331*, 1420.
[60] C. T. Nelson, B. Winchester, Y. Zhang, S.-J. Kim, A. Melville, C. Adamo, C. M. Folkman, S.-H. Baek, C.-B. Eom, D. G. Schlom, *Nano Lett.* **2011**, *11*, 828.
[61] Y. Ivry, D. P. Chu, J. F. Scott, C. Durkan, *Phys. Rev. Lett.* **2010**, *104*, 207602.
[62] R. K. Vasudevan, Y. C. Chen, H. H. Tai, N. Balke, P. P. Wu, S. Bhattacharya, L. Q. Chen, Y. H. Chu, I. N. Lin, S. V. Kalinin, V. Nagarajan, *ACS Nano* **2011**, *5*, 879.
[63] Y. L. Tang, Y. L. Zhu, X. L. Ma, A. Y. Borisevich, A. N. Morozovska, E. A. Eliseev, W. Y. Wang, Y. J. Wang, Y. B. Xu, Z. D. Zhang, S. J. Pennycook, *Science* **2015**, *348*, 547.
[64] R. G. P. McQuaid, L. J. McGilly, P. Sharma, A. Gruverman, J. M. Gregg, *Nat. Commun.* **2011**, *2*, 404.
[65] N. Balke, S. Choudhury, S. Jesse, M. Huijben, Y. H. Chu, A. P. Baddorf, L. Q. Chen, R. Ramesh, S. V. Kalinin, *Nat. Nanotechnol.* **2009**, *4*, 868.
[66] S. C. Chae, Y. Horibe, D. Y. Jeong, S. Rodan, N. Lee, S.-W. Cheong, *Proc. Natl. Acad. Sci. USA* **2010**, *107*, 21366.
[67] Y. J. Qi, Z. H. Chen, C. W. Huang, L. H. Wang, X. D. Han, J. L. Wang, P. Yang, T. Sritharan, L. Chen, *J. Appl. Phys.* **2012**, *111*, 104117.
[68] Z. Li, Y. Wang, G. Tian, P. Li, L. Zhao, F. Zhang, J. Yao, H. Fan, X. Song, D. Chen, Z. Fan, M. Qin, M. Z. Zeng, Z. Zhang, X. Lu, S. Hu, C. Lei, Q. Zhu, J. Li, X. Gao, J.-M. Liu, *Sci. Adv.* **2017**, *3*, e1700919.
[69] A. K. Yadav, C. T. Nelson, S. L. Hsu, Z. Hong, J. D. Clarkson, C. M. Schlepuetz, A. R. Damodaran, P. Shafer, E. Arenholz, L. R. Dedon, D. Chen, A. Vishwanath, A. M. Minor, L. Q. Chen, J. F. Scott, L. W. Martin, R. Ramesh, *Nature* **2016**, *530*, 198.
[70] K.-E. Kim, S. Jeong, K. Chu, J. H. Lee, G.-Y. Kim, F. Xue, T. Y. Koo, L.-Q. Chen, S.-Y. Choi, R. Ramesh, C.-H. Yang, *Nat. Commun.* **2018**, *9*, 403.
[71] B. J. Rodriguez, X. S. Gao, L. F. Liu, W. Lee, I. I. Naumov, A. M. Bratkovsky, D. Hesse, M. Alexe, *Nano Lett.* **2009**, *9*, 1127.
[72] X.-K. Wei, C.-L. Jia, T. Sluka, B.-X. Wang, Z.-G. Ye, N. Setter, *Nat. Commun.* **2016**, *7*, 12385.
[73] S. Cherifi-Hertel, H. Bulou, R. Hertel, G. Taupier, K. D. H. Dorkenoo, C. Andreas, J. Guyonnet, I. Gaponenko, K. Gallo, P. Paruch, *Nat. Commun.* **2017**, *8*, 15768.
[74] G. De Luca, M. D. Rossell, J. Schaab, N. Viart, M. Fiebig, M. Trassin, *Adv. Mater.* **2017**, *29*, 1605145.
[75] J. Ma, J. Ma, Q. Zhang, R. Peng, J. Wang, C. Liu, M. Wang, N. Li, M. Chen, X. Cheng, P. Gao, L. Gu, L.-Q. Chen, P. Yu, J. Zhang, C.-W. Nan, *Nat. Nanotechnol.* **2018**, *13*, 947.
[76] M. J. Han, Y. J. Wang, Y. L. Tang, Y. L. Zhu, J. Y. Ma, W. R. Geng, M. J. Zou, Y. P. Feng, N. B. Zhang, X. L. Ma, *J. Phys. Chem. C* **2019**, *123*, 2557.
[77] Y. Nahas, S. Prokhorenko, J. Fischer, B. Xu, C. Carretero, S. Prosandeev, M. Bibes, S. Fusil, B. Dkhil, V. Garcia, L. Bellaiche, *Nature* **2020**, *577*, 47.
[78] Q. Zhang, L. Xie, G. Liu, S. Prokhorenko, Y. Nahas, X. Pan, L. Bellaiche, A. Gruverman, N. Valanoor, *Adv. Mater.* **2017**, *29*, 1702375.
[79] J. J. P. Peters, G. Apachitei, R. Beanland, M. Alexe, A. M. Sanchez, *Nat. Commun.* **2016**, *7*, 13484.
[80] N. Choudhury, L. Walizer, S. Lisenkov, L. Bellaiche, *Nature* **2011**, *470*, 513.
[81] L. Li, X. Cheng, J. R. Jokisaari, P. Gao, J. Britson, C. Adamo, C. Heikes, D. G. Schlom, L.-Q. Chen, X. Pan, *Phys. Rev. Lett.* **2018**, *120*, 137602.
[82] Y. Nahas, S. Prokhorenko, L. Louis, Z. Gui, I. Kornev, L. Bellaiche, *Nat. Commun.* **2015**, *6*, 8542.
[83] S. Das, Y. L. Tang, Z. Hong, M. A. P. Goncalves, M. R. McCarter, C. Klewe, K. X. Nguyen, F. Gomez-Ortiz, P. Shafer, E. Arenholz, V. A. Stoica, S. L. Hsu, B. Wang, C. Ophus, J. F. Liu, C. T. Nelson, S. Saremi, B. Prasad, A. B. Mei, D. G. Schlom, J. Iniguez, P. Garcia-Fernandez, D. A. Muller, L. Q. Chen, J. Junquera, L. W. Martin, R. Ramesh, *Nature* **2019**, *568*, 368.
[84] E. Bousquet, M. Dawber, N. Stucki, C. Lichtensteiger, P. Hermet, S. Gariglio, J.-M. Triscone, P. Ghosez, *Nature* **2008**, *452*, 732.
[85] D. A. Tenne, A. Bruchhausen, N. D. Lanzillotti-Kimura, A. Fainstein, R. S. Katiyar, A. Cantarero, A. Soukiassian,

V. Vaithyanathan, J. H. Haeni, W. Tian, D. G. Schlom, K. J. Choi, D. M. Kim, C. B. Eom, H. P. Sun, X. Q. Pan, Y. L. Li, L. Q. Chen, Q. X. Jia, S. M. Nakhmanson, K. M. Rabe, X. X. Xi, *Science* **2006**, *313*, 1614.
[86] Y. Gu, M. Li, A. N. Morozovska, Y. Wang, E. A. Eliseev, V. Gopalan, L.-Q. Chen, *Phys. Rev. B* **2014**, *89*, 174111.
[87] U. K. Rossler, A. N. Bogdanov, C. Pfleiderer, *Nature* **2006**, *442*, 797.
[88] N. Balke, B. Winchester, W. Ren, Y. H. Chu, A. N. Morozovska, E. A. Eliseev, M. Huijben, R. K. Vasudevan, P. Maksymovych, J. Britson, S. Jesse, I. Kornev, R. Ramesh, L. Bellaiche, L. Q. Chen, S. V. Kalinin, *Nat. Phys.* **2012**, *8*, 81.
[89] P. Shafer, P. Garcia-Fernandez, P. Aguado-Puente, A. R. Damodaran, A. K. Yadav, C. T. Nelson, S. L. Hsu, J. C. Wojdel, J. Iniguez, L. W. Martin, E. Arenholz, J. Junquera, R. Ramesh, *Proc. Natl. Acad. Sci. USA* **2018**, *115*, 915.
[90] L. Van Lich, T. Shimada, J. Wang, V.-H. Dinh, T. Q. Bui, T. Kitamura, *Phys. Rev. B* **2017**, *96*, 134119.
[91] P. Zubko, J. C. Wojdel, M. Hadjimichael, S. Fernandez-Pena, A. Sene, I. Luk'yanchuk, J.-M. Triscone, J. Iniguez, *Nature* **2016**, *534*, 524.
[92] A. K. Yadav, K. X. Nguyen, Z. J. Hong, P. Garcia-Fernandez, P. Aguado-Puente, C. T. Nelson, S. Das, B. Prasad, D. Kwon, S. Cheema, A. I. Khan, C. M. Hu, J. Iniguez, J. Junquera, L. Q. Chen, D. A. Muller, R. Ramesh, S. Salahuddin, *Nature* **2019**, *565*, 468.
[93] H. Y. Hwang, Y. Iwasa, M. Kawasaki, B. Keimer, N. Nagaosa, Y. Tokura, *Nat. Mater.* **2012**, *11*, 103.
[94] F. Zheng, F. N. Rybakov, A. B. Borisov, D. Song, S. Wang, Z.-A. Li, H. Du, N. S. Kiselev, J. Caron, A. Kovacs, *Nat. Nanotechnol.* **2018**, *13*, 451.
[95] M. Ezawa, *Phys. Rev. Lett.* **2010**, *105*, 197202.
[96] I. Dzyaloshinsky, *J. Phys. Chem. Solids* **1958**, *4*, 241.
[97] T. Moriya, *Phys. Rev.* **1960**, *120*, 91.
[98] A. Leonov, M. Mostovoy, *Nat. Commun.* **2015**, *6*, 8275.
[99] X. Zhang, J. Xia, Y. Zhou, X. Liu, H. Zhang, M. Ezawa, *Nat. Commun.* **2017**, *8*, 1717.
[100] S. Rohart, A. Thiaville, *Phys. Rev. B* **2013**, *88*, 184422.
[101] Y. Tokunaga, X. Yu, J. White, H. M. Rønnow, D. Morikawa, Y. Taguchi, Y. Tokura, *Nat. Commun.* **2015**, *6*, 7638.
[102] S. Woo, K. Litzius, B. Krüger, M.-Y. Im, L. Caretta, K. Richter, M. Mann, A. Krone, R. M. Reeve, M. Weigand, P. Agrawa, I. Lemesh, M.-A. Mawass, P. Fischer, M. Kläui, G. S. D. Beach, *Nat. Mater.* **2016**, *15*, 501.
[103] L. Caretta, M. Mann, F. Büttner, K. Ueda, B. Pfau, C. M. Günther, P. Hessing, A. Churikova, C. Klose, M. Schneider, *Nat. Nanotechnol.* **2018**, *13*, 1154.
[104] D. Liang, J. P. DeGrave, M. J. Stolt, Y. Tokura, S. Jin, *Nat. Commun.* **2015**, *6*, 8217.
[105] F. Büttner, I. Lemesh, M. Schneider, B. Pfau, C. M. Günther, P. Hessing, J. Geilhufe, L. Caretta, D. Engel, B. Krüger, *Nat. Nanotechnol.* **2017**, *12*, 1040.
[106] S. Woo, K. M. Song, X. Zhang, Y. Zhou, M. Ezawa, X. Liu, S. Finizio, J. Raabe, N. J. Lee, S.-I. Kim, *Nat. Commun.* **2018**, *9*, 959.
[107] D. Maccariello, W. Legrand, N. Reyren, K. Garcia, K. Bouzehouane, S. Collin, V. Cros, A. Fert, *Nat. Nanotechnol.* **2018**, *13*, 233.
[108] A. Hrabec, J. Sampaio, M. Belmeguenai, I. Gross, R. Weil, S. M. Chérif, A. Stashkevich, V. Jacques, A. Thiaville, S. Rohart, *Nat. Commun.* **2017**, *8*, 15765.
[109] G. Yu, P. Upadhyaya, X. Li, W. Li, S. K. Kim, Y. Fan, K. L. Wong, Y. Tserkovnyak, P. K. Amiri, K. L. Wang, *Nano Lett.* **2016**, *16*, 1981.
[110] J. Iwasaki, M. Mochizuki, N. Nagaosa, *Nat. Nanotechnol.* **2013**, *8*, 742.
[111] F. Jonietz, S. Mühlbauer, C. Pfleiderer, A. Neubauer, W. Münzer, A. Bauer, T. Adams, R. Georgii, P. Böni, R. A. J. S. Duine, *Science* **2010**, *330*, 1648.
[112] W. Wang, Y. Zhang, G. Xu, L. Peng, B. Ding, Y. Wang, Z. Hou, X. Zhang, X. Li, E. Liu, *Adv. Mater.* **2016**, *28*, 6887.
[113] W. Jiang, X. Zhang, G. Yu, W. Zhang, X. Wang, M. B. Jungfleisch, J. E. Pearson, X. Cheng, O. Heinonen, K. L. Wang, *Nat. Phys.* **2017**, *13*, 162.
[114] Y. Li, N. Kanazawa, X. Yu, A. Tsukazaki, M. Kawasaki, M. Ichikawa, X. Jin, F. Kagawa, Y. Tokura, *Phys. Rev. Lett.* **2013**, *110*, 117202.
[115] F. Hellman, A. Hoffmann, Y. Tserkovnyak, G. S. D. Beach, E. E. Fullerton, C. Leighton, A. H. MacDonald, D. C. Ralph, D. A. Arena, H. A. Durr, P. Fischer, J. Grollier, J. P. Heremans, T. Jungwirth, A. V. Kimel, B. Koopmans, I. N. Krivorotov, S. J. May, A. K. Petford-Long, J. M. Rondinelli, N. Samarth, I. K. Schuller, A. N. Slavin, M. D. Stiles, O. Tchernyshyov, A. Thiaville, B. L. Zink, *Rev. Mod. Phys.* **2017**, *89*, 025006.
[116] T. H. R. Skyrme, *Nucl. Phys.* **1962**, *31*, 556.
[117] A. N. Bogdanov, D. Yablonskii, *Sov. Phys. JETP* **1989**, *95*, 178.
[118] A. Bogdanov, A. Hubert, *J. Magn. Magn. Mater.* **1994**, *138*, 255.
[119] A. Bogdanov, U. Rößler, *Phys. Rev. Lett.* **2001**, *87*, 037203.
[120] H. Du, R. Che, L. Kong, X. Zhao, C. Jin, C. Wang, J. Yang, W. Ning, R. Li, C. Jin, *Nat. Commun.* **2015**, *6*, 8504.
[121] N. Romming, C. Hanneken, M. Menzel, J. E. Bickel, B. Wolter, K. von Bergmann, A. Kubetzka, R. Wiesendanger, *Science* **2013**, *341*, 636.
[122] C. Moreau-Luchaire, C. Moutafis, N. Reyren, J. Sampaio, C. Vaz, N. Van Horne, K. Bouzehouane, K. Garcia, C. Deranlot, P. Warnicke, P. Wohlhüter, J.-M. George, M. Weigand, J. Raabe, V. Cros, A. Fert, *Nat. Nanotechnol.* **2016**, *11*, 444.
[123] O. Boulle, J. Vogel, H. Yang, S. Pizzini, D. de Souza Chaves, A. Locatelli, T. O. Menteş, A. Sala, L. D. Buda-Prejbeanu, O. Klein, M. Belmeguenai, Y. Roussigné, A. Stashkevich, S. M. Chérif, L. Aballe, M. Foerster, M. Chshiev, S. Auffret, I. M. Miron, G. Gaudin, *Nat. Nanotechnol.* **2016**, *11*, 449.
[124] A. Soumyanarayanan, M. Raju, A. G. Oyarce, A. K. Tan, M.-Y. Im, A. P. Petrović, P. Ho, K. Khoo, M. Tran, C. Gan, *Nat. Mater.* **2017**, *16*, 898.
[125] L. Wang, C. Liu, N. Mehmood, G. Han, Y. Wang, X. Xu, C. Feng, Z. Hou, Y. Peng, X. Gao, *ACS Appl. Mater. Interfaces* **2019**, *11*, 12098.
[126] L. Sun, R. Cao, B. Miao, Z. Feng, B. You, D. Wu, W. Zhang, A. Hu, H. Ding, *Phys. Rev. Lett.* **2013**, *110*, 167201.
[127] J. Li, A. Tan, K. W. Moon, A. Doran, M. A. Marcus, A. T. Young, E. Arenholz, S. Ma, R. F. Yang, C. Hwang, Z. Q. Qiu, *Nat. Commun.* **2014**, *5*, 4704.
[128] D. A. Gilbert, B. B. Maranville, A. L. Balk, B. J. Kirby, P. Fischer, D. T. Pierce, J. Unguris, J. A. Borchers, K. Liu, *Nat. Commun.* **2015**, *6*, 8462.
[129] Z. Hou, W. Ren, B. Ding, G. Xu, Y. Wang, B. Yang, Q. Zhang, Y. Zhang, E. Liu, F. Xu, *Adv. Mater.* **2017**, *29*, 1701144.
[130] Z. P. Hou, B. Zhang, G. Z. Xu, S. F. Zhang, C. Gong, B. Ding, H. Li, F. Xu, Y. Yao, E. K. Liu, G. H. Wu, X. X. Zhang, W. H. Wang, *ACS Nano* **2019**, *13*, 922.
[131] T. Kurumaji, T. Nakajima, M. Hirschberger, A. Kikkawa, Y. Yamasaki, H. Sagayama, H. Nakao, Y. Taguchi, T.-H. Arima, Y. Tokura, *Science* **2019**, *365*, 914.
[132] X. Zhang, Y. Zhou, M. Ezawa, *Nat. Commun.* **2016**, *7*, 10293.
[133] T. Dohi, S. DuttaGupta, S. Fukami, H. Ohno, *Nat. Commun.* **2019**, *10*, 5153.
[134] J. Barker, O. A. Tretiakov, *Phys. Rev. Lett.* **2016**, *116*, 147203.
[135] X. C. Zhang, Y. Zhou, M. Ezawa, *Sci. Rep.* **2016**, *6*, 24795.
[136] J. Zang, M. Mostovoy, J. H. Han, N. Nagaosa, *Phys. Rev. Lett.* **2011**, *107*, 136804.

[137] C. D. Jin, C. K. Song, J. B. Wang, Q. F. Liu, *Appl. Phys. Lett.* **2016**, *109*, 182404.
[138] B. Gobel, A. Mook, J. Henk, I. Mertig, *Phys. Rev. B* **2017**, *96*, 060406.
[139] L. Smejkal, Y. Mokrousov, B. H. Yan, A. H. MacDonald, *Nat. Phys.* **2018**, *14*, 242.
[140] G. Q. Yu, P. Upadhyaya, Q. M. Shao, H. Wu, G. Yin, X. Li, C. L. He, W. J. Jiang, X. F. Han, P. K. Amiri, K. L. Wang, *Nano Lett.*. **2017**, *17*, 261.
[141] S. S. Parkin, M. Hayashi, L. Thomas, *Science* **2008**, *320*, 190.
[142] Z. Hou, Q. Zhang, X. Zhang, G. Xu, J. Xia, B. Ding, H. Li, S. Zhang, N. M. Batra, P. M. Costa, *Adv. Mater.* **2019**, 1904815.
[143] P.-J. Hsu, A. Kubetzka, A. Finco, N. Romming, K. von Bergmann, R. Wiesendanger, *Nat. Nanotechnol.* **2017**, *12*, 123.
[144] M. Schott, A. Bernand-Mantel, L. Ranno, S. Pizzini, J. Vogel, H. Béa, C. Baraduc, S. Auffret, G. Gaudin, D. Givord, *Nano Lett.* **2017**, *17*, 3006.
[145] C. Ma, X. Zhang, J. Xia, M. Ezawa, W. Jiang, T. Ono, S. Piramanayagam, A. Morisako, Y. Zhou, X. Liu, *Nano Lett.* **2019**, *19*, 353.
[146] Y. Nii, T. Nakajima, A. Kikkawa, Y. Yamasaki, K. Ohishi, J. Suzuki, Y. Taguchi, T. Arima, Y. Tokura, Y. Iwasa, *Nat. Commun.* **2015**, *6*, 8539.
[147] S.-G. Je, P. Vallobra, T. Srivastava, J.-C. Rojas-Sánchez, T. H. Pham, M. Hehn, G. Malinowski, C. Baraduc, S. Auffret, G. Gaudin, *Nano Lett.* **2018**, *18*, 7362.
[148] X. Zhang, W. Cai, X. Zhang, Z. Wang, Z. Li, Y. Zhang, K. Cao, N. Lei, W. Kang, Y. Zhang, *ACS Appl. Mater. Interfaces* **2018**, *10*, 16887.
[149] S. Kasai, S. Sugimoto, Y. Nakatani, R. Ishikawa, Y. K. Takahashi, *Appl. Phys. Express* **2019**, *12*, 083001.
[150] A. Soumyanarayanan, N. Reyren, A. Fert, C. Panagopoulos, *Nature* **2016**, *539*, 509.
[151] N. Kanazawa, Y. Onose, T. Arima, D. Okuyama, K. Ohoyama, S. Wakimoto, K. Kakurai, S. Ishiwata, Y. Tokura, *Phys. Rev. Lett.* **2011**, *106*, 156603.
[152] A. Neubauer, C. Pfleiderer, B. Binz, A. Rosch, R. Ritz, P. Niklowitz, P. Böni, *Phys. Rev. Lett.* **2009**, *102*, 186602.
[153] M. Raju, A. Yagil, A. Soumyanarayanan, A. K. Tan, A. Almoalem, F. Ma, O. Auslaender, C. Panagopoulos, *Nat. Commun.* **2019**, *10*, 696.
[154] Y. Ohuchi, J. Matsuno, N. Ogawa, Y. Kozuka, M. Uchida, Y. Tokura, M. Kawasaki, *Nat. Commun.* **2018**, *9*, 213.
[155] L. Vistoli, W. Wang, A. Sander, Q. Zhu, B. Casals, R. Cichelero, A. Barthélémy, S. Fusil, G. Herranz, S. Valencia, R. Abrudan, E. Weschke, K. Nakazawa, H. Kohno, J. Santamaria, W. Wu, V. Garcia, M. Bibes, *Nat. Phys.* **2019**, *15*, 67.
[156] Q. Qin, L. Liu, W. Lin, X. Shu, Q. Xie, Z. Lim, C. Li, S. He, G. M. Chow, J. Chen, *Adv. Mater.* **2019**, *31*, 1807008.
[157] L. Wang, Q. Feng, Y. Kim, R. Kim, K. H. Lee, S. D. Pollard, Y. J. Shin, H. Zhou, W. Peng, D. Lee, W. Meng, H. Yang, J. H. Han, M. Kim, Q. Lu, T. W. Noh, *Nat. Mater.* **2018**, *17*, 1087.
[158] X. Li, W. V. Liu, L. Balents, *Phys. Rev. Lett.* **2014**, *112*, 067202.
[159] S. Huang, C. Chien, *Phys. Rev. Lett.* **2012**, *108*, 267201.
[160] S. Chakraverty, T. Matsuda, H. Wadati, J. Okamoto, Y. Yamasaki, H. Nakao, Y. Murakami, S. Ishiwata, M. Kawasaki, Y. Taguchi, *Phys. Rev. B* **2013**, *88*, 220405.
[161] C. Sürgers, G. Fischer, P. Winkel, H. v. Löhneysen, *Nat. Commun.* **2014**, *5*, 3400.
[162] Y. Cheng, S. Yu, M. Zhu, J. Hwang, F. Yang, *Phys. Rev. Lett.* **2019**, *123*, 237206.
[163] Y. Taguchi, Y. Oohara, H. Yoshizawa, N. Nagaosa, Y. Tokura, *Science* **2001**, *291*, 2573.
[164] D. Xiao, M.-C. Chang, Q. Niu, *Rev. Mod. Phys.* **2010**, *82*, 1959.
[165] F. Haldane, *Phys. Rev. Lett.* **2004**, *93*, 206602.
[166] Q. Shao, Y. Liu, G. Yu, S. K. Kim, X. Che, C. Tang, Q. L. He, Y. Tserkovnyak, J. Shi, K. L. Wang, *Nat. Electron.* **2019**, *2*, 182.
[167] Y. Ohuchi, Y. Kozuka, M. Uchida, K. Ueno, A. Tsukazaki, M. Kawasaki, *Phys. Rev. B* **2015**, *91*, 245115.
[168] N. Mohanta, E. Dagotto, S. Okamoto, *Phys. Rev. B* **2019**, *100*, 064429.
[169] Y. Li, L. Zhang, Q. Zhang, C. Li, T. Yang, Y. Deng, L. Gu, D. Wu, *ACS Appl. Mater. Interfaces* **2019**, *11*, 21268.
[170] M. Uchida, M. Kawasaki, *J. Phys. D: Appl. Phys.* **2018**, *51*, 143001.
[171] B. Sohn, B. Kim, S. Y. Park, H. Y. Choi, J. Y. Moon, T. Choi, Y. J. Choi, T. W. Noh, H. Zhou, S. H. Chang, arXiv:1810.01615, **2018**.
[172] Z. Li, S. Shen, Z. Tian, K. Hwangbo, M. Wang, Y. Wang, F. M. Bartram, L. He, Y. Lyu, Y. Dong, G. Wan, H. Li, N. Lu, J. Zang, H. Zhou, E. Arenholz, Q. He, L. Yang, W. Luo, P. Yu, *Nat. Commun.* **2020**, *11*, 184.
[173] H. Wang, Y. Y. Dai, Z. R. Liu, Q. D. Xie, C. Liu, W. N. Lin, L. Liu, P. Yang, J. Wang, T. V. Venkatesan, G. M. Chow, H. Tian, Z. D. Zhang, J. S. Chen, *Adv. Mater.* **2020**, *32*, 1904415.
[174] D. Kan, T. Moriyama, K. Kobayashi, Y. Shimakawa, *Phys. Rev. B* **2018**, *98*, 180408.
[175] L. Wu, Y. Zhang, arXiv:1812.09847, **2018**.
[176] D. J. Groenendijk, C. Autieri, T. C. van Thiel, W. Brzezicki, N. Gauquelin, P. Barone, K. H. van den Bos, S. van Aert, J. Verbeeck, A. Filippetti, S. Picozzi, M. Cuoco, A. D. Caviglia, arXiv:1810.05619, **2018**.
[177] W. Wang, M. W. Daniels, Z. Liao, Y. Zhao, J. Wang, G. Koster, G. Rijnders, C. Z. Chang, D. Xiao, W. Wu, *Nat. Mater.* **2019**, *18*, 1054.
[178] L. Wu, F. Wen, Y. Fu, J. H. Wilson, X. Liu, Y. Zhang, D. M. Vasiukov, M. S. Kareev, J. Pixley, J. Chakhalian, arXiv:1907.07579, **2019**.
[179] P.-C. Wu, H. Song, Y. Yuan, B. Feng, Y. Ikuhara, R. Huang, P. Yu, C.-G. Duan, Y.-H. Chu, *Phys. Rev. Mater.* **2020**, *4*, 014401.
[180] G. Malsch, D. Ivaneyko, P. Milde, L. Wysocki, L. Yang, P. H. van Loosdrecht, I. Lindfors-Vrejoiu, L. M. Eng, *ACS Appl. Nano Mater.* **2020**, *3*, 1182.
[181] L. Wang, Q. Feng, H. G. Lee, E. K. Ko, Q. Lu, T. W. Noh, *Nano Lett.* **2020**, *20*, 2468.
[182] I. Lindfors-Vrejoiu, M. Ziese, *Phys. Status Solidi B* **2017**, *254*, 1600556.
[183] M. Nakamura, D. Morikawa, X. Yu, F. Kagawa, T.-H. Arima, Y. Tokura, M. Kawasaki, *J. Phys. Soc. Jpn.* **2018**, *87*, 074704.
[184] R. J. Xu, J. Karthik, A. R. Damodaran, L. W. Martin, *Nat. Commun.* **2014**, *5*, 3120.
[185] S. Liu, R. E. Cohen, *Phys. Rev. B* **2017**, *95*, 094102.
[186] Y. L. Wang, A. K. Tagantsev, D. Damjanovic, N. Setter, *Appl. Phys. Lett.* **2007**, *91*, 062905.
[187] W. N. Lawless, J. Fousek, *J. Phys. Soc. Jpn.* **1970**, *28*, 419.
[188] S. Wada, K. Yako, K. Yokoo, H. Kakemoto, T. Tsurumi, *Ferroelectrics* **2006**, *334*, 17.
[189] A. N. Morozovska, E. A. Eliseev, O. V. Varenyk, S. V. Kalinin, *J. Appl. Phys.* **2013**, *113*, 187222.
[190] Z. Yuan, J. Ruan, L. Xie, X. Pan, D. Wu, P. Wang, *Appl. Phys. Lett.* **2017**, *110*, 171602.
[191] W. Gao, C. Addiego, H. Wang, X. Yan, Y. Hou, D. Ji, C. Heikes, Y. Zhang, L. Li, H. Huyan, T. Blum, T. Aoki, Y. Nie, D. G. Schlom, R. Wu, X. Pan, *Nature* **2019**, *575*, 480.
[192] Y. L. Tang, Y. L. Zhu, Y. J. Wang, W. Y. Wang, Y. B. Xu, W. J. Ren, Z. D. Zhang, X. L. Ma, *Sci. Rep.* **2015**, *4*, 4115.
[193] Y. L. Tang, Y. L. Zhu, X. L. Man, *Ultramicroscopy* **2016**, *160*, 57.
[194] Y. Liu, Y. L. Tang, Y. L. Zhu, W. Y. Wang, X. L. Ma, *Adv. Mater. Interfaces* **2016**, *3*, 1600342.
[195] B. Meyer, D. Vanderbilt, *Phys. Rev. B* **2002**, *65*, 104111.

[196] D. Lee, R. K. Behera, P. Wu, H. Xu, Y. Li, S. B. Sinnott, S. R. Phillpot, L. Chen, V. Gopalan, *Phys. Rev. B* **2009**, *80*, 060102.
[197] M. Taherinejad, D. Vanderbilt, P. Marton, V. Stepkova, J. Hlinka, *Phys. Rev. B* **2012**, *86*, 155138.
[198] T. Rojac, A. Bencan, G. Drazic, N. Sakamoto, H. Ursic, B. Jancar, G. Tavcar, M. Makarovic, J. Walker, B. Malic, *Nat. Mater.* **2017**, *16*, 322.
[199] M. Schröder, A. Haußmann, A. Thiessen, E. Soergel, T. Woike, L. M. Eng, *Adv. Funct. Mater.* **2012**, *22*, 3936.
[200] T. Sluka, A. K. Tagantsev, P. Bednyakov, N. Setter, *Nat. Commun.* **2013**, *4*, 1808.
[201] D. Meier, J. Seidel, A. Cano, K. Delaney, Y. Kumagai, M. Mostovoy, N. A. Spaldin, R. Ramesh, M. Fiebig, *Nat. Mater.* **2012**, *11*, 284.
[202] J. Guyonnet, I. Gaponenko, S. Gariglio, P. Paruch, *Adv. Mater.* **2011**, *23*, 5377.
[203] S. Farokhipoor, B. Noheda, *Phys. Rev. Lett.* **2011**, *107*, 127601.
[204] Y. Xiao, V. B. Shenoy, K. Bhattacharya, *Phys. Rev. Lett.* **2005**, *95*, 247603.
[205] J. A. Mundy, J. Schaab, Y. Kumagai, A. Cano, M. Stengel, I. P. Krug, D. Gottlob, H. Doğanay, M. E. Holtz, R. Held, *Nat. Mater.* **2017**, *16*, 622.
[206] P. Sharma, Q. Zhang, D. Sando, C. H. Lei, Y. Y. Liu, J. Y. Li, V. Nagarajan, J. Seidel, *Sci. Adv.* **2017**, *3*, e1700512.
[207] J. Jiang, Z. L. Bai, Z. H. Chen, L. He, D. W. Zhang, Q. H. Zhang, J. A. Shi, M. H. Park, J. F. Scott, C. S. Hwang, *Nat. Mater.* **2018**, *17*, 49.
[208] J. Seidel, D. Fu, S.-Y. Yang, E. Alarcón-Lladó, J. Wu, R. Ramesh, J. W. Ager III, *Phys. Rev. Lett.* **2011**, *107*, 126805.
[209] A. Bhatnagar, A. R. Chaudhuri, Y. H. Kim, D. Hesse, M. Alexe, *Nat. Commun.* **2013**, *4*, 2835.
[210] M. Alexe, D. Hesse, *Nat. Commun.* **2011**, *2*, 256.
[211] T. Choi, S. Lee, Y. J. Choi, V. Kiryukhin, S.-W. Cheong, *Science* **2009**, *324*, 63.
[212] B. Guzelturk, A. B. Mei, L. Zhang, L. Z. Tan, P. Donahue, A. G. Singh, D. G. Schlom, L. W. Martin, A. M. Lindenberg, *Nano Lett.* **2020**, *20*, 145.
[213] S. Salahuddin, S. Datta, *Nano Lett.* **2008**, *8*, 405.
[214] J. Iniguez, P. Zubko, I. Luk'yanchuk, A. Cano, *Nat. Rev. Mater.* **2019**, *4*, 243.
[215] Z. Q. Gu, S. Pandya, A. Samanta, S. Liu, G. Xiao, C. J. G. Meyers, A. R. Damodaran, H. Barak, A. Dasgupta, S. Saremi, A. Polemi, L. Y. Wu, A. A. Podpirka, A. Will-Cole, C. J. Hawley, P. K. Davies, R. A. York, I. Grinberg, L. W. Martin, J. E. Spanier, *Nature* **2018**, *560*, 622.
[216] G. Arlt, U. Bottger, S. Witte, *Ann. Phys.* **1994**, *506*, 578.
[217] L. McGilly, P. Yudin, L. Feigl, A. Tagantsev, N. Setter, *Nat. Nanotechnol.* **2015**, *10*, 145.
[218] X. Lu, Z. Chen, Y. Cao, Y. Tang, R. Xu, S. Saremi, Z. Zhang, L. You, Y. Dong, S. Das, H. Zhang, L. Zheng, H. Wu, W. Lv, G. Xie, X. Liu, J. Li, L. Chen, L.-Q. Chen, W. Cao, L. W. Martin, *Nat. Commun.* **2019**, *10*, 3951.
[219] R. Wang, D. Fong, F. Jiang, M. Highland, P. Fuoss, C. Thompson, A. Kolpak, J. Eastman, S. Streiffer, A. Rappe, G. Stephenson, *Phys. Rev. Lett.* **2009**, *102*, 047601.
[220] S. Matzen, O. Nesterov, G. Rispens, J. Heuver, M. Biegalski, H. Christen, B. Noheda, *Nat. Commun.* **2014**, *5*, 4415.
[221] I. Stolichnov, L. Feigl, L. J. McGilly, T. Sluka, X.-K. Wei, E. Colla, A. Crassous, K. Shapovalov, P. Yudin, A. K. Tagantsev, N. Setter, *Nano Lett.* **2015**, *15*, 8049.
[222] F. Rubio-Marcos, A. Del Campo, P. Marchet, J. F. Fernandez, *Nat. Commun.* **2015**, *6*, 6594.
[223] S. Farokhipoor, C. Magén, S. Venkatesan, J. Íñiguez, C. J. Daumont, D. Rubi, E. Snoeck, M. Mostovoy, C. De Graaf, A. Müller, M. Döblinger, C. Scheu, B. Noheda, *Nature* **2014**, *515*, 379.
[224] Q. He, C.-H. Yeh, J.-C. Yang, G. Singh-Bhalla, C.-W. Liang, P.-W. Chiu, G. Catalan, L. Martin, Y.-H. Chu, J. Scott, R. Ramesh, *Phys. Rev. Lett.* **2012**, *108*, 067203.
[225] L. W. Martin, Y.-H. Chu, M. B. Holcomb, M. Huijben, P. Yu, S.-J. Han, D. Lee, S. X. Wang, R. Ramesh, *Nano Lett.* **2008**, *8*, 2050.
[226] H. Béa, M. Bibes, F. Ott, B. Dupé, X.-H. Zhu, S. Petit, S. Fusil, C. Deranlot, K. Bouzehouane, A. Barthélémy, *Phys. Rev. Lett.* **2008**, *100*, 017204.
[227] Z. Chen, J. Liu, Y. Qi, D. Chen, S.-L. Hsu, A. R. Damodaran, X. He, A. T. N'Diaye, A. Rockett, L. W. Martin, *Nano Lett.* **2015**, *15*, 6506.
[228] J. Y. Chauleau, T. Chirac, S. Fusil, V. Garcia, W. Akhtar, J. Tranchida, P. Thibaudeau, I. Gross, C. Blouzon, A. Finco, M. Bibes, B. Dkhil, D. D. Khalyavin, P. Manuel, V. Jacques, N. Jaouen, M. Viret, *Nat. Mater.* **2020**, *19*, 386.
[229] J. Seidel, P. Maksymovych, Y. Batra, A. Katan, S.-Y. Yang, Q. He, A. P. Baddorf, S. V. Kalinin, C.-H. Yang, J.-C. Yang, Y.-H. Chu, E. K. H. Salje, H. Wormeester, M. Salmeron, R. Ramesh, *Phys. Rev. Lett.* **2010**, *105*, 197603.
[230] M. Y. Gureev, A. K. Tagantsev, N. Setter, *Phys. Rev. B* **2011**, *83*, 184104.
[231] P. Maksymovych, A. N. Morozovska, P. Yu, E. A. Eliseev, Y. H. Chu, R. Ramesh, A. P. Baddorf, S. V. Kalinin, *Nano Lett.* **2012**, *12*, 209.
[232] Y. S. Oh, X. Luo, F. T. Huang, Y. Z. Wang, S. W. Cheong, *Nat. Mater.* **2015**, *14*, 407.
[233] E. A. Eliseev, A. N. Morozovska, G. S. Svechnikov, V. Gopalan, V. Y. Shur, *Phys. Rev. B* **2011**, *83*, 235313.
[234] A. Crassous, T. Sluka, A. K. Tagantsev, N. Setter, *Nat. Nanotechnol.* **2015**, *10*, 614.
[235] P. Maksymovych, *Nat. Nanotechnol.* **2015**, *10*, 571.
[236] P. Bednyakov, T. Sluka, A. Tagantsev, D. Damjanovic, N. Setter, *Adv. Mater.* **2016**, *28*, 9498.
[237] G. Tian, W. D. Yang, X. Song, D. F. Zheng, L. Y. Zhang, C. Chen, P. L. Li, H. Fan, J. X. Yao, D. Y. Chen, Z. Fan, Z. P. Hou, Z. Zhang, S. J. Wu, M. Zeng, X. S. Gao, J. M. Liu, *Adv. Funct. Mater.* **2019**, *29*, 1807276.
[238] C. S. Werner, S. J. Herr, K. Buse, B. Sturman, E. Soergel, C. Razzaghi, I. Breunig, *Sci. Rep.* **2017**, *7*, 9862.
[239] S. Van Aert, S. Turner, R. Delville, D. Schryvers, G. Van Tendeloo, E. K. H. Salje, *Adv. Mater.* **2012**, *24*, 523.
[240] T. Zykova-Timan, E. K. H. Salje, *Appl. Phys. Lett.* **2014**, *104*, 082907.
[241] D. V. Christensen, Y. Frenkel, Y. Z. Chen, Y. W. Xie, Z. Y. Chen, Y. Hikita, A. Smith, L. Klein, H. Y. Hwang, N. Pryds, B. Kalisky, *Nat. Phys.* **2019**, *15*, 269.
[242] M. Honig, J. A. Sulpizio, J. Drori, A. Joshua, E. Zeldov, S. Ilani, *Nat. Mater.* **2013**, *12*, 1112.
[243] B. Kalisky, E. M. Spanton, H. Noad, J. R. Kirtley, K. C. Nowack, C. Bell, H. K. Sato, M. Hosoda, Y. W. Xie, Y. Hikita, C. Woltmann, G. Pfanzelt, R. Jany, C. Richter, H. Y. Hwang, J. Mannhart, K. A. Moler, *Nat. Mater.* **2013**, *12*, 1091.
[244] A. Aird, E. K. H. Salje, *J. Phys.: Condens. Matter* **1998**, *10*, L377.
[245] J. F. Scott, E. K. H. Salje, M. A. Carpenter, *Phys. Rev. Lett.* **2012**, *109*, 187601.
[246] E. K. H. Salje, M. Alexe, S. Kustov, M. C. Weber, J. Schiemer, G. F. Nataf, J. Kreisel, *Sci. Rep.* **2016**, *6*, 27193.
[247] E. K. H. Salje, J. F. Scott, *Appl. Phys. Lett.* **2014**, *105*, 252904.
[248] V. Stepkova, P. Marton, J. Hlinka, *Phys. Rev. B* **2015**, *92*, 094106.
[249] S. R. Zhang, Y. L. Zhu, Y. L. Tang, Y. Liu, S. Li, M. J. Han, J. Y. Ma, B. Wu, Z. H. Chen, S. Saremi, X. L. Ma, *Adv. Mater.* **2017**, *29*, 1703543.
[250] Y. L. Tang, Y. L. Zhu, X. L. Ma, Z. J. Hong, Y. J. Wang, W. Y. Wang, Y. B. Xu, Y. Liu, B. Wu, L. Chen, C. W. Huang, L. Q. Chen, Z. H. Chen, H. J. Wu, S. J. Pennycook, *Adv. Funct. Mater.* **2019**, *29*, 1901687.
[251] C.-L. Jia, S.-B. Mi, K. Urban, I. Vrejoiu, M. Alexe, D. Hesse, *Nat. Mater.* **2008**, *7*, 57.

[252] Y. Liu, Y.-J. Wang, Y.-L. Zhu, C.-H. Lei, Y.-L. Tang, S. Li, S.-R. Zhang, J. Li, X.-L. Ma, *Nano Lett.* **2017**, *17*, 7258.
[253] Y. L. Tang, Y. L. Zhu, Y. Liu, Y. J. Wang, X. L. Ma, *Nat. Commun.* **2017**, *8*, 15994.
[254] Z. Hong, A. R. Damodaran, F. Xue, S.-L. Hsu, J. Britson, A. K. Yadav, C. T. Nelson, J.-J. Wang, J. F. Scott, L. W. Martin, *Nano Lett.* **2017**, *17*, 2246.
[255] V. A. Stoica, N. Laanait, C. Dai, Z. Hong, Y. Yuan, Z. Zhang, S. Lei, M. R. McCarter, A. Yadav, A. R. Damodaran, S. Das, G. A. Stone, J. Karapetrova, D. A. Walko, X. Zhang, L. W. Martin, R. Ramesh, L. Q. Chen, H. Wen, V. Gopalan, J. W. Freeland, *Nat. Mater.* **2019**, *18*, 377.
[256] A. R. Damodaran, J. Clarkson, Z. Hong, H. Liu, A. Yadav, C. Nelson, S.-L. Hsu, M. McCarter, K.-D. Park, V. Kravtsov, A. Farhan, Y. Dong, Z. Cai, H. Zhou, P. Aguado-Puente, P. García-Fernández, J. Íñiguez, J. Junquera, A. Scholl, M. B. Raschke, L.-Q. Chen, D. D. Fong, R. Ramesh, L. W. Martin, *Nat. Mater.* **2017**, *16*, 1003.
[257] H. Callen, R. M. Josephs, *J. Appl. Phys.* **1971**, *42*, 1977.
[258] B. K. Lai, I. Ponomareva, I. I. Naumov, I. Kornev, H. X. Fu, L. Bellaiche, G. J. Salamo, *Phys. Rev. Lett.* **2006**, *96*, 137602.
[259] Q. Zhang, S. Prokhorenko, Y. Nahas, L. Xie, L. Bellaiche, A. Gruverman, N. Valanoor, *Adv. Funct. Mater.* **2019**, *29*, 1808573.
[260] Z. Hong, L.-Q. Chen, *Acta Mater.* **2018**, *152*, 155.
[261] M. A. P. Goncalves, C. Escorihuela-Sayalero, P. Garca-Fernandez, J. Junquera, J. Iniguez, *Sci. Adv.* **2019**, *5*, eaau7023.
[262] M. W. Tate, P. Purohit, D. Chamberlain, K. X. Nguyen, R. Hovden, C. S. Chang, P. Deb, E. Turgut, J. T. Heron, D. G. Schlom, *Microsc. Microanal.* **2016**, *22*, 237.
[263] P. García-Fernández, J. C. Wojdeł, J. Íñiguez, J. Junquera, *Phys. Rev. B* **2016**, *93*, 195137.
[264] A. Fert, V. Cros, J. Sampaio, *Nat. Nanotechnol.* **2013**, *8*, 152.
[265] R. Tomasello, E. Martinez, R. Zivieri, L. Torres, M. Carpentieri, G. Finocchio, *Sci. Rep.* **2015**, *4*, 6784.
[266] I. Luk'yanchuk. Y. Tikhonov. A. Razumnaya, V. M. Vinokur, arXiv:1907.03866, **2019**.
[267] Y. Tikhonov, S. Kondovych, J. Mangeri, M. Pavlenko, L. Baudry, A. Sené, A. Galda, S. Nakhmanson, O. Heinonen, A. Razumnaya, I. Luk'yanchuk, V. M. Vinokur, arXiv:2001.01790, **2020**.
[268] M. P. Warusawithana, E. V. Colla, J. N. Eckstein, M. B. Weissman, *Phys. Rev. Lett.* **2003**, *90*, 036802.